# Acknowledgement

Before expressing my gratitude to all those who gave me the possibility to complete this thesis, I would like to dedicate this dissertation to my beloved parents and my sisters and brother who always have faith in me and give me their endless love.

I am deeply indebted to my supervisor Prof. Katsuaki Koike from Kyoto University whose supervision, stimulating suggestions, patience and encouragement benefit me all the time of research. This dissertation could not have been finished without his persistent guidance. I believe the academic spirit on Prof. Koike will influence my whole research career.

My grateful thank also goes to my second supervisor Prof. Jun Shimada whose supervision and warm caring give me courage for completing the dissertation. I am also heartily appreciating the valuable comments from my committee, Morimura sensei, Takio sensei and Asaue sensei. I also wish to thank to Prof. Bin Gu from Sichuan University for his caring and valuable comments on my research.

I would like to thank to all members in the Laboratory of Applied Geosciences and Technology, Kumamoto University, especially Dr. Alaa, Yoshinaga san, Aixiangu shijie, Akune san, Togesaka san, Yoshida san, Misonou san, Suetsugu san, Kubo san, Ha-jie and others.

Especially, I would like to give my special thanks to my husband Bingwei Tian whose patient love enabled me to complete this research. Also, I would like to thank to all my friends for their caring and encouragement.

Last but not least I owe my gratefulness to my motherland, China, for awarding me scholarship which makes my study possible. I also sincerely thank to Kumamoto University for providing such great environment for my research and study.

Sincerely

WANG Ling

# Abstract

This dissertation aims to clarify spatial-temporal vegetation pattern associated with fracture zone by combining techniques of remote sensing, geographic information system (GIS), geostatistics and landscape ecology.

Vegetation pattern appears different characteristics across different scale. Factors that influence the pattern are scale dependence. At a global scale, vegetation pattern is dependent on solar radiation, climate and temperature. At a local scale, small scale, topography becomes a dominant factor controlling vegetation distribution because it can reallocate locally water and solar radiation. However, fracture zones including faults, gouges and continuous joints may influence the vegetation pattern more strongly than topography by changing hydraulic conductivity and other soil properties around the fracture zone. In particular, vegetation patterns such as alignment of the same vegetation type may be formed by fracture zones that control groundwater flow and produce various soil types by strong weathering processes. Accordingly, the distribution of vegetation is expected to correlate with the fracture zone, which is the main focus of this dissertation.

A suitable study area, situated near the epicenter of the Wenchuan earthquake, was selected for the purposes of this study. Initially, a segment tracing algorithm (STA) method was applied for identifying the regional fracture system through lineament extractions from a shaded digital elevation model with 25 m mesh. Additionally, a lineament density map was produced to characterize the heterogeneity of lineament distribution by counting the number of centers of lineaments per km2. Three major fracture zones were detected from the dense zones of the interpreted fractures, which corresponded with Pitiaohe, Gengda and Yingxiu Faults from northwest to southeast, by referring to a geological structure map of

Sichuan province and literature from state forestry administration, R.R. China. The strikes of these three fracture zones are N30-50°E.

The destruction of vegetation caused by the Wenchuan earthquake was revealed from change of NDVI values of ETM+ images before and after the earthquake. The ruined distribution of vegetations was clarified to be generally consistent with the fracture zones by comparing ruined distribution map with the lineament density map.

To examine the distribution of vegetation types and its relationship to fracture zones, vegetation cover map was firstly made by applying a hybrid unsupervised-supervised approach to advanced land observing satellite (ALOS) image. Seven categories of the main vegetation types were defined: evergreen broad-leaved forest; deciduous broad-leaved forest; deciduous and evergreen broad-leaved forest; coniferous forest; meadow; farmland; shrub and the other class, such as snow, ice, and water body, which was unrelated to vegetation. Distribution areas of each vegetation type were combined with the graded lineament density which was defined based on the quartile of cumulative distribution to examine the positional relationship between the vegetation pattern and the fracture zones. Moreover, anisotropy of NDVI semivariogram was used to examine whether the fracture zones affected the vegetation trend. According to the results, forests persisted in the less fractured areas, while farmlands relatively tend to persist in fractured areas with high level. On the other hand, anisotropy results revealed that vegetation pattern tend to be more continuous along the strikes of fracture zones, which indicated that fracture zones have certain impacts on forming vegetation pattern.

Previous work focused on vegetation distribution and its change pattern associated with fracture zones. A further research aims at quantifying the special heterogeneity

change of vegetation pattern, because we not only have to detect change, but also have to determine the magnitude and rate of change. Geostatistics and landscape metrics were employed to quantify the spatial heterogeneity of vegetation pattern in numerical and categorical map, respectively. NDVI semivariogram reveals the variability and structure change of vegetation pattern. Landscape metrics depicts the composition and configuration changes of vegetation pattern.

Remote sensing, GIS, geostatistics techniques were well applied in this dissertation. Remote sensing and GIS have been wide used in landscape ecology, however, the application of geostatistics in ecology have been not penetrated deeply. The combination of remote sensing and geostatistics for characterizing vegetation pattern associated with fracture zones is a new research in vegetation ecology, which is bound to be brand view in this field.

# Contents

# List of tables

# Lists of figures

# Chapter 1

# Introduction

## 1.1 Background

Vegetation is an important part of the landscape. Assemblages of species of plants constitute vegetation. Vegetation type, in terms of its structure and its functioning, is dependent on the environment; on the other hand, it also can influence the environment. The environment is integration of interaction of physical factor, chemical factor and biotic factor. In general, the environment encompasses climate, soil, topography and humans (Qu, 1984).

Vegetation is worldwide different. Variation in climate is a major factor that determines the way vegetation varies around the world. Plants have two suites of climatic limits. Most obvious and most frequently detected are the limits on growth. Equally important, but perhaps less frequently realized, are the absolute limits of survival (Beerling and Woodward, 2001). For plants in seasonal climates there may be one or more periods of the year in which growth is not possible, generally because of limiting temperatures or precipitation. At high latitudes there are periods of the year in which the sun does not appear above the horizon and so photosynthesis would be impossible, even if temperatures were appropriate for growth. Plants may either endure or avoid such periods. Endurance is characterized by plants showing little growth or activity but retaining all obvious productive characters such as green leaves and living roots. Avoidance is characteristic by very marked changes in plants, seen particularly as leaf abscission and the death of fine roots. Once the environment again becomes suitable for growth, plants will develop new and active leaves and roots. Even plants which are evergreen endures tend to progress through periods of new development and repair at this transition to the growing season.

Whittaker (1960) (who popularized the Five Kingdom classification system) noted that the major vegetation types of the world are substantially predicted by two primary climatic variables: mean annual temperature and total annual precipitation. A simplified version of a diagram with these two axes and the various major biomes mapped onto it is shown in Fig.1.1

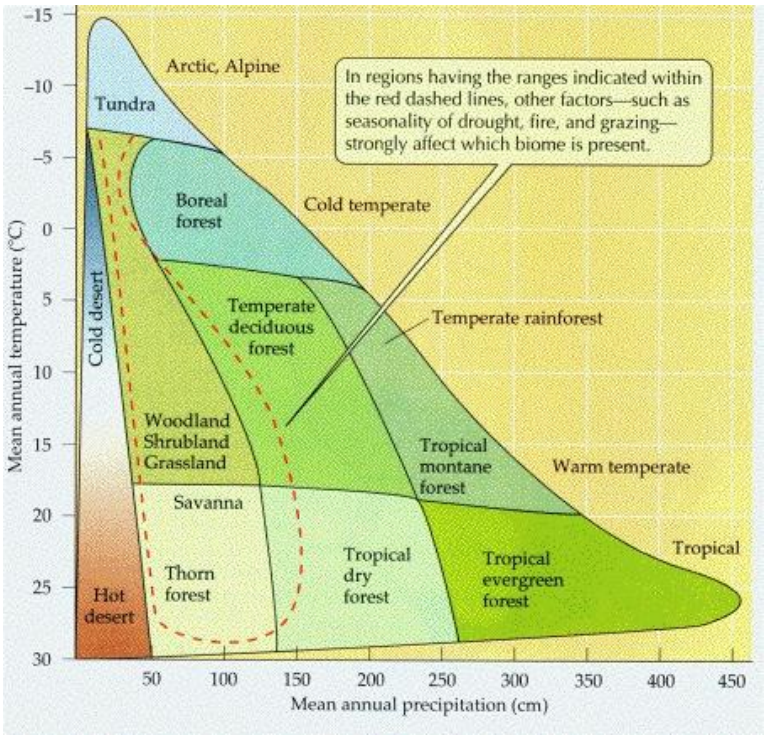


Fig. 1.1. Diagram of major biomes corresponding to mean annual temperature and mean annual precipitation

Climate and vegetation are related so closed that the classifications of climate have often been developed on the basis of conditions of plants. A well-known instance is Köppen-Geiger climate classification (Peel et al., 2007) (Fig.1.1). Köppen described vegetation as “crystallized, visible climate” and referred to it as being an indicator of

climate that is much more accurate than instruments. In other words, vegetation is as being so completely determined by climate as to be a perfect climate indicator.

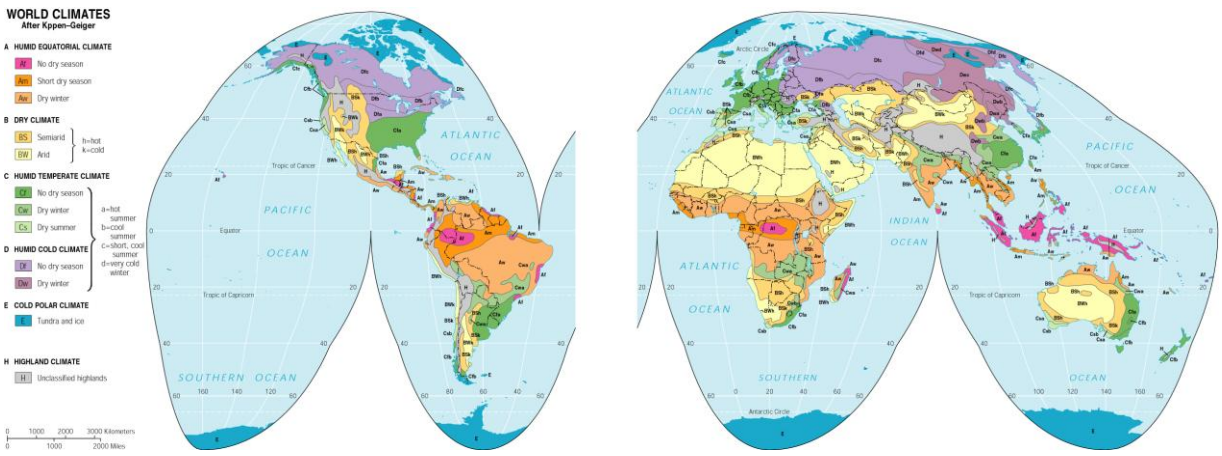


Fig. 1.2. World climate after Kppen-Geiger

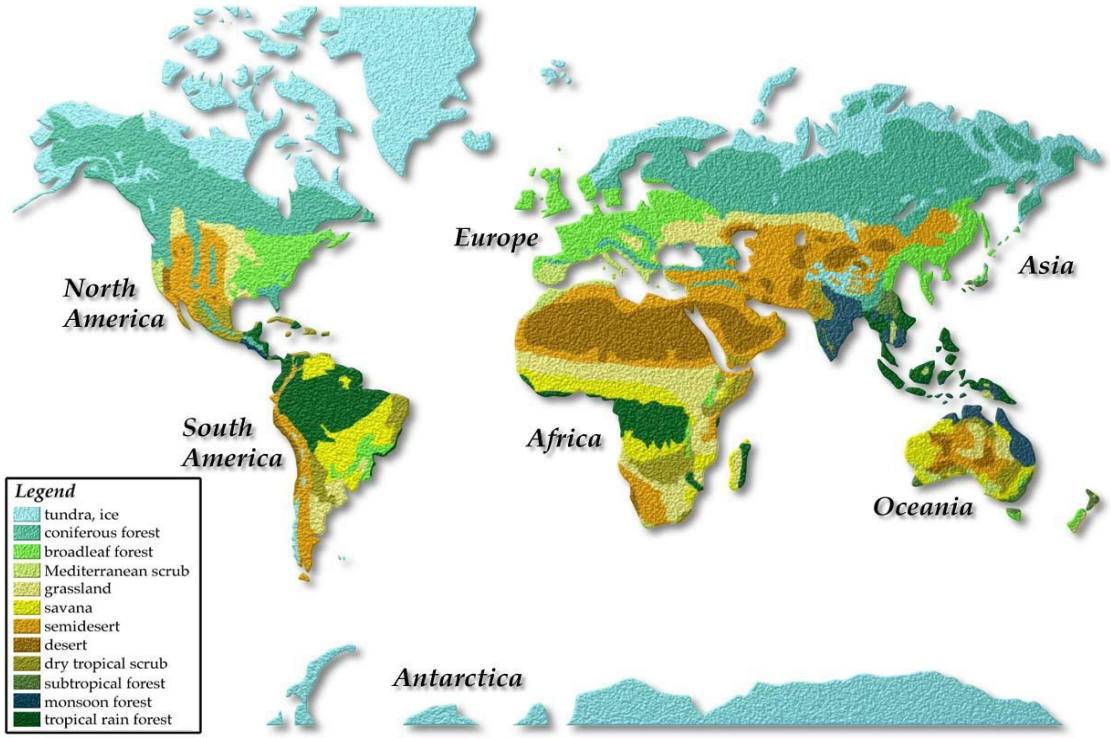


Fig. 1.3. World vegetation map

Figure 1.3 displays vegetation map in the world, which indicate that vegetation patterns are strongly recall that of climate (Fig.1.2).

Climate determines the vegetation type in global scale. However, in regional zone, the specific distribution of vegetation is more affected by soil and topography (Qu, 1984). For instance, it is supposed to be covered by evergreen broad-leaved forest in Shanghai according to the condition of climate; there is indeed such vegetation in Yunxi area of Shanghai where yellow brown soil exists; however, salinized meadow can be found living nearby where seashore saline soil is dominant. Such examples are too numerous to mention individually.

Topography, including elevation, aspect, slope, also have impact on the distribution of vegetation. However, topography itself does not have the direct influence on vegetation; it indirectly affects the distribution of vegetation by changing the local climate (Fig1.4) and soil conditions (Hara et al., 1996). Take the elevation as an example, vegetation in the foot of mountain is quite different from that in the top of mountain; Temperature, Humidity, soil composition, and solar radiation are distinct. Local climate is affected by anything else that moves the air mass up and down or affects its water-load, such as mountain ranges. As a relatively moist, moving, air mass hits high mountains, it is forced to rise, gets cooler, and the moisture condenses, dropping rain on the lower and mid slopes of the windward side of the mountain-range. As the air descends on the other side, it gets warmer, and its moisture debt increases. Fig1.4 depicts how vegetation recalls the local climate affected by mountain ranges.

In other cases, humans have much influence on the vegetation. Humans have cleared away much of the world's natural plant cover, and replaced it with fields and

buildings, or forest plantations of trees from other parts of the world. In other instances the vegetation is a sort of hybrid of human influence and nature; battered by fires or by grazing animals, and yet still distinctive to its region.

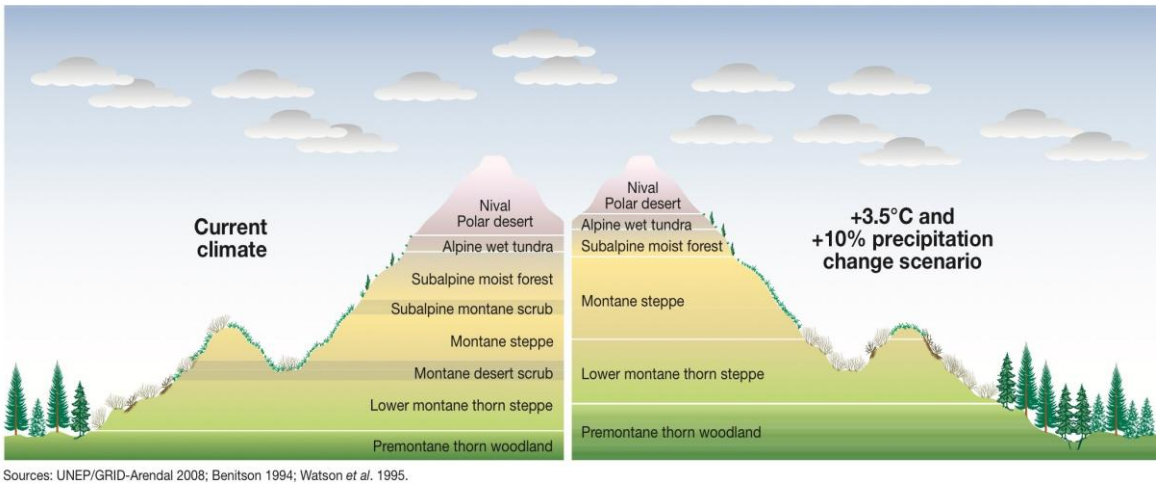


Fig. 1.4. Local climate impact on mountain vegetation zones

As with almost everything in nature, there is a combination of reasons why things are the way they are. We listed many reasons that could influence the distribution of vegetations that have been proofed by many researchers. In this research, we propose to understand the relationship between vegetation and fracture zones in detail.

Fracture zones have received less consideration than other environmental factors related to vegetation distribution. One reason might be that fracture zones are not as easily characterized as the other environmental factors. Fracture zones are generally concealed by thick surficial deposits, which make the estimation difficult. In addition, conventional lineament extraction techniques, which commonly based on visual interpretation and hand-tracing of linear features depicted on aerial photographs or paper-based satellite image mosaics, are time-consuming, tedious, subjective and irreproducible. Although main faults

that can be comparatively easy recognized in the field have been received much attention, main fracture is not a single plane containing filling materials, but is mostly accompanied by damage zone involving subordinate fractures and, in some cases, bounded by belts of anomalously low densities and seismic velocities zone extending a few kilometers. Fracture systems in the region are still under poorly characterized.

Nevertheless, fracture zones were considered to have effect on the distribution of vegetation. Fracture zones are believed to act as conduits for transporting the subsurface ground flow (Ruland et al., 1991). Moreover, fracture zones, formed by fracturing and chemical alteration, must have larger permeability than that of the surrounding rocks and emphasize the importance of themselves as major flow paths. On the other hand, fracture zones might influence the property of soil around them by strong weathering processes. Accordingly, we assumed that fracture zones might have indirect effect on the vegetation pattern by controlling ground water flow and producing various soil types.

Related work on the relationship between fracture zones and vegetation were limited. Informed study always focused on well-known faults (Robbins, 1958; Vogl and McHargue, 1996). Accordingly, a detail characteristic of fracture zones and their relationship to vegetation pattern are expected examined.

Another major work implemented in this research is characterizing the earthquake-induced vegetation change pattern and clarifying its relationship to the fracture zone. The study area selected in this research is around the epicenter of Wenchuan earthquake, which destroyed a large amount of natural forest. The earthquake also induced secondary mountain disasters such as landslide, rock falls, collapse, debris flows, barrier lakes, which ruined the vegetation sequentially. Landslide is one of the most important events causing

vegetation pattern change after a large earthquake because it converts vegetation cover into bare area. The landslides were mostly concentrated in two areas, near the seismogenic fault and on the steep slopes adjacent to the Minjiang River (Huang et al., 2008; Chigira et al., 2010; Tang et al., 2010; Fan et al., 2010). However, except for several representative active faults such as the Longmenshan fracture zones, the regional changes of vegetation pattern induced by an earthquake and their relationships with fracture zones have not been examined in detail. Accordingly, analysis of relationship between earthquake-induced vegetation change pattern and local fracture zones is necessary for characterizing the damage distribution of vegetation after the earthquake.

The final main part of the dissertation focuses on the quantification of spatial heterogeneity of vegetation and its change during the earthquake. Spatial heterogeneity is considered by several authors to be the single most important factor regulating the distribution of species (Wiens 1976; Urban et al., 1987; Pollock et al., 1998; Huston 1994). Risser (1987) defines spatial heterogeneity as the degree of dissimilarity over a given extent. Landscape heterogeneity, defined by the degree of spatial heterogeneity, is heavily influenced by geomorphology and topography (Pastor et al., 1982; Swanson et al., 1988). Finally, vegetation heterogeneity, which is directly related to landscape heterogeneity, is the degree of dissimilarity of species distribution over a given extent. Given these definitions, vegetation heterogeneity is controlled by landscape heterogeneity. Especially, in alpine area, vegetation heterogeneity can even represent landscape heterogeneity, since the structure of alpine environment is often characterized by assessing the pattern and composition of plant productivity and cover type information (Brown, 1994; Walsh et al., 1994)

Quantification of spatial heterogeneity is a promising way of examining structure of ecological systems. Spatial heterogeneity is considered to have great effects on functions and processes of ecological systems and these changes in spatial heterogeneity may reflect changes in functions and processes (Li, 1994). The disturbances of Wenchuan earthquake consequently destructed the ecosystem by ruining a large amount of forest. To monitor ecosystem changes after and before the earthquake at landscape scale, we design to quantify the spatial heterogeneity change of vegetation.

## 1.2 Objectives

The emphasis of this research was placed on the relationship between vegetation pattern and fracture zones. Initially, characteristics of fracture zone in the study area were required. The strike, dip and density of fracture zones need to be well examined. Moreover, existence of faults, which could influence the environment where vegetation lives more intensively, should be clarified.

Another key point is vegetation pattern. We need to examine the following questions. How many kinds of vegetation exist in the study area? How about the distribution of such vegetations? What is the change pattern of vegetations like induced by the earthquake?

Previous ones are the basis objectives of this research. Since our study focuses on the relationship between vegetation pattern and fracture zones, we intend to solve the following problems. Firstly, relationship between earthquake-induced vegetation change and distribution of fracture zones are required to be clarified; then, vegetation distribution

and its relationship to fracture zones is expected to be examined; indeed, quantification of spatial heterogeneity of vegetation, a complement for vegetation pattern, is indispensable.

## 1.3 Outline of Dissertation

Chapter 1 is the introduction of this research. Background and objectives of this study were presented. Relationship between vegetation and environment is the biggest issue in vegetation ecology.

Chapter 2 describes the study area in terms of the location, geology, and other environmental characters. A big event, the Wenchuan earthquake, which occurred in this area, is introduced. Meanwhile, in this chapter, main methodologies utilized through this dissertation, remote sensing, geographic information systems, geostatistics and landscape ecology, were presented; e.g. their principles, advantages and relationship between each other. In the final part of this chapter, the data sources used to realize our objectives were listed.

Chapter 3 characterizing the distribution of fracture zones in terms of lineament extracted by segment tracing algorithm. NDVI based vegetation change were detected to examine the change pattern induced by Wenchuan earthquake and further to clarify the relationship of it relevant to the distribution of fracture zones.

The emphasis of chapter 4 is placed on the relationship between vegetation distribution and fracture zones. Techniques of remote sensing and geography information system are integrated to make vegetation classification map. NDVI semivariograms are employed to analyze the relationship between vegetation alignments related to fracture zones.

Chapter 5 focuses on the quantification of spatial heterogeneous of vegetation and analysis of dynamically change of vegetation pattern before and after the earthquake. Landscape metrics are utilized to quantify the spatial heterogeneity of vegetation for categorical map. On the other hand, Geostatic technique is considered as method for numerical map.

Chapter 6 summarizes the conclusion of each chapter. Main results will be presented in this chapter. In addition, future work will also be mentioned.

## Reference


Beerling, D., Woodward, F., 2001. Vegetation and the terrestrial carbon cycle: modeling the first 400 million years. Cambridge University Press. 23-96.

Brown, D., Danial, G., 1994. Predicting vegetation types at tree line using topography and biophysical disturbance. Journal of Vegetation Science, 5:641-656.

Chigira, M., Wu, X., Inokuchi, T., Wang, G., 2010. Landslides induced by the 2008 Wenchuan earthquake, Sichuan, China. Geomorphology, 118: 225-238.

Fan, J., Chen, J., Tian, B., 2010. Rapid assessment of secondary disasters induced by the Wenchuan earthquake. Computing in Science & Engineering, 12(1):10-19.

Hara, M., Hirata, K., Fujihara, M., and Oono, K., 1996. Vegetation structure in relation to micro-landform in an evergreen broad-leaved forest on Amami Ohshima Island, Southwest Japan. Ecological Research, 11:325-337.

Huang, R., Li, W., 2008. Development and distribution of geohazards triggered by 5.12 Wenchuan earthquakes in China. Science in China Series E: Technical Science, 52:810-819.

Huston, M., 1994. Biological Diversity. Cambridge University Press. Cambridge.

Pastor, J., Aber, J., Mcclaugherty, C., and Melillo, J., 1982. Geology, Soils and Vegetation of Blackhawk Island, Wisconsin. The American Midland Naturalist. 108:266-277.

Peel, M. C., Finlayson, B. L., and McMahon, T., 2007. Updated world map of the Kppen-Geiger climate classification, Hydrol. Earth Syst. Sci., 11: 1633–1644.

Pollock, M., Naiman, R., and Hanley, T., 1998. Plant species richness in riparian wetlands-a test of biodiversity theory. Ecology, 79(1): 94-105.

Qu, Z., 1984. Plant Ecology. Higher Education Press, Beijing, 45-50.

Risser, P., 1987. Landscape ecology: state of the art. Landscape Heterogeneity and Disturbance, 3-14.

Robbins, R., 1958. Direct effect of the 1855 earthquake on the vegetation of the Orongorongo Valley, Wellington. Transactions of the Royal Society of New Zealand, 85(2):205-212.

Ruland, W., Cherry, J., Feenstra, S., 1991. The depth of fractures and active ground-water flow in a clayey till plain in south-western ontario. Ground Water, 29(3): 405-417.

Swanson, F., Kratz, T., Caine, N., and Woodmansee, R., 1988. Landform effects on ecosystem pattern and processes. Bioscience, 38(2): 92-98.

Tang, H., Jia, H., Hu, X., Li, D., Xiong, C., 2010. Characteristics of landslides induced by the great Wenchuan earthquake. Journal of Earth Science, 21: 104-113.

Urban, D., O'Neil, R., and Shugart, H., 1987. Landscape ecology. Bioscience, 37:119-127.

Vogl, R. and McHargue, L., 1996. Vegetation of California Fan Palm Oases on the San Andreas Fault. Ecology, 47(4), 532-540.

Whittaker, R. H. 1960. Vegetation of the Siskiyou Mountains, Oregon and California. Ecological Monographs 30:279–338.

Wiens, J., 1976. Population responses to patchy environments. Annual Review of Ecology and Systematics, 7: 81-120.

# Chapter 2

# Study Area and Methodology

## 2.1 Study Area

### 2.1.1 Whenchuan earthquake

A destructive earthquake of magnitude 8.0 Ms according to the China Earthquake Administration and 7.9 Mw according to the US Geological Survey struck the Longmeng Shan region of Sichuan Province, China at 14:28 on 12 May 2008. This earthquake, named the Wenchuan earthquake because the location of its epicenter was in the administrative region of Wenchuan County, was located in Yingxiu town about 80 km west-northwest of Chengdu, the capital of Sichuan. The coordinates of the epicenter were 31.021° N and 103.367° E and its focal depth was 15 km. It caused a great amount of damage to infrastructure as well as causing human fatalities. It also induced large-scale landslides and debris flows, silting rivers and barrier lakes. Moreover, the earthquake-induced secondary mountain disasters are geological disasters trigged by earthquake and aftershocks in a mountain areas, such as landslide, rock falls, collapse, avalanche (snow or ice landslide), debris flows, barrier lakes (including landslide-dammed lake, avalanche-dammed lake and debris flow-dammed lake), mountain torrents, land subsidence, ground fissure, water loss and soil erosion. The Whenchuan earthquake and aftershocks induced large quantities of secondary mountain disasters with causing new casualties and damage after the main shock.

The main shock and seriously destructed area by the earthquake mainly include 12 counties, namely Wenchuan, Beichuan, Qingchuan, Anxian, Pingwu, Maoxian, Dujiangyan, Jiangyou, Pengzhou, Shifang, Mianzhu, and Chongzhou. The earthquake was occurred on the Longmen Shan fault zone that separate the Sichuan basin from the eastern

margin of the Tibetan plateau. The Longmen Shan fault zone is composed of three major sub-parallel faults: the Pengguan fault (PGF) in the east along the mountain front, the Beichuan fault (BCF) about 10-15km west to the PGF, and the Wenchuan-Maoxian (WMF) fault about another 30km west of the BCF (Fig. 2.1). The tectonic zone of the Longmen Shan fault extends along NE-SW with a length of 300 km and width of 50-70 km. The main shock was initiated on the BCF about 30km southwest of Yingxiu, and propagated unilaterally northeastward. The main shock area was an alpine and canyon region with increasing elevations from southeast to northwest. Such geomorphology of the study area tends to induce mountain hazards, in special landslides and debris flows.

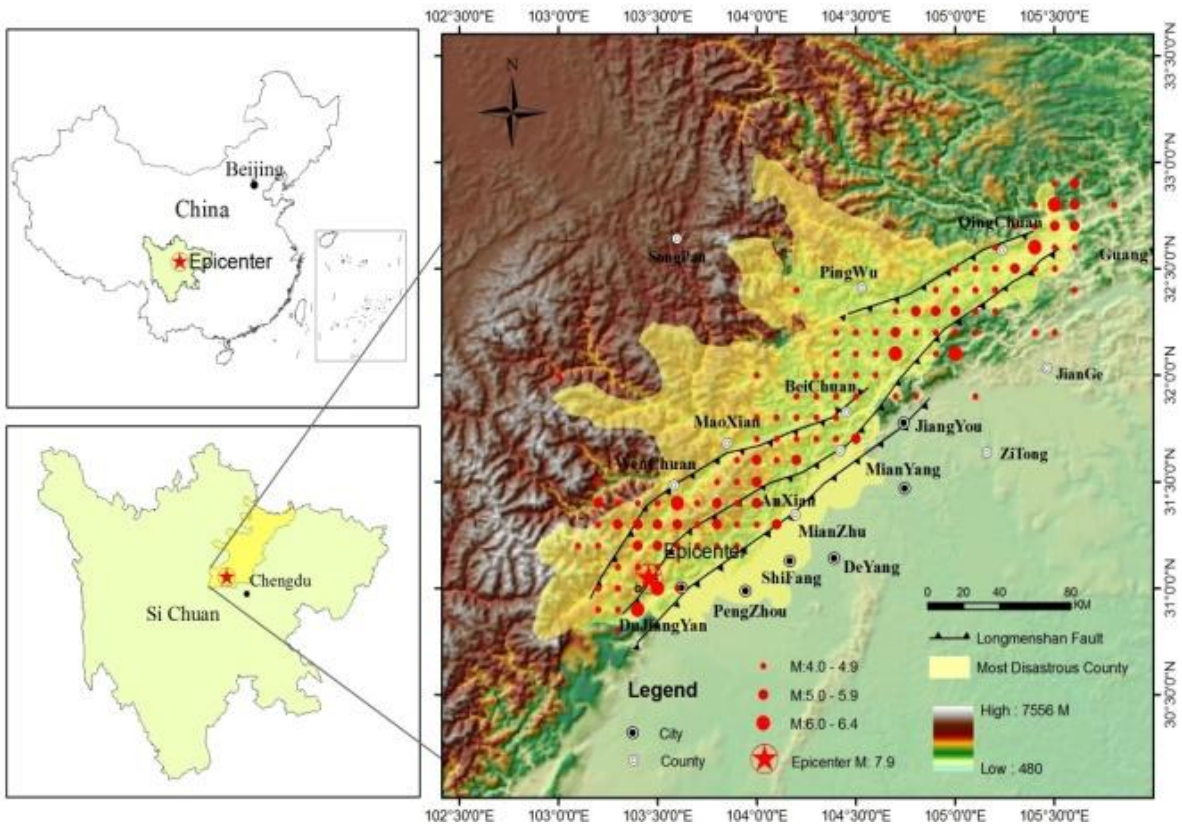


Fig. 2.1. The main shock area of Whenchuan Earthquake

Landslides triggered by the Wenchuan earthquake were mostly concentrated in two areas, near the seismogenic fault and on the steep slopes adjacent to the Min River (Huang et al., 2008; Chigira et al., 2010; Tang et al., 2010; Fan et al., 2010). The Min River is a first-order tributary of the Yangtze River. The accordant junction of two rivers is located in Yibin city. Min River is not only of economical but also ecological significance in southwestern China. It is the main water resource in Sichuan Province. The Wenchuan earthquake destroyed a large amount of natural forest around the Min River basin, which is to some extent influencing the ecosystem in local.

### 2.1.2 Location of study area

Study area is located in the south of Upper Min River Basin, including Yinxiu town, Wolong Nature Reserve and Sanjiang Reserve, which is situated near the epicenter of the Wenchuan earthquake (Fig. 2.2). This area supplies water and ecological protection services to the dry valley of upper Minjiang River, which has various land-use types. However, it is also a typical ecologically fragile area of western China.

The study area covers 66 $km^2$ and contains two watersheds, Yuzixi and Shouxi, which are the two main tributaries of the Min River. Yuzixi River originates from Mt. Balang with a flow direction from southwest to northeast, total length of 89 km, and basin areas of 1742 $km^2$. It passes through Wolong Nature Reserve and Yinxiu town and finally flows into Min River. Shouxi River has its source in Mt. Menkan. It flows through Sanjiang Nature Reserve, Shuimo town and Xuankou town into Min River, and has a total length of 65 km and area of 596 $km^2$.

The study area is generally mountainous, as shown by the digital elevation model (DEM) in Fig. 2.2, with high mountains over 6000 m a.s.l. such as Mt. Siguniang (6250 m). Pitiao River acts as a boundary of the topographic shape of the study area: the topography is entirely high in the northwest side of Pitiao River, while the topography becomes gentle in its southeast side.

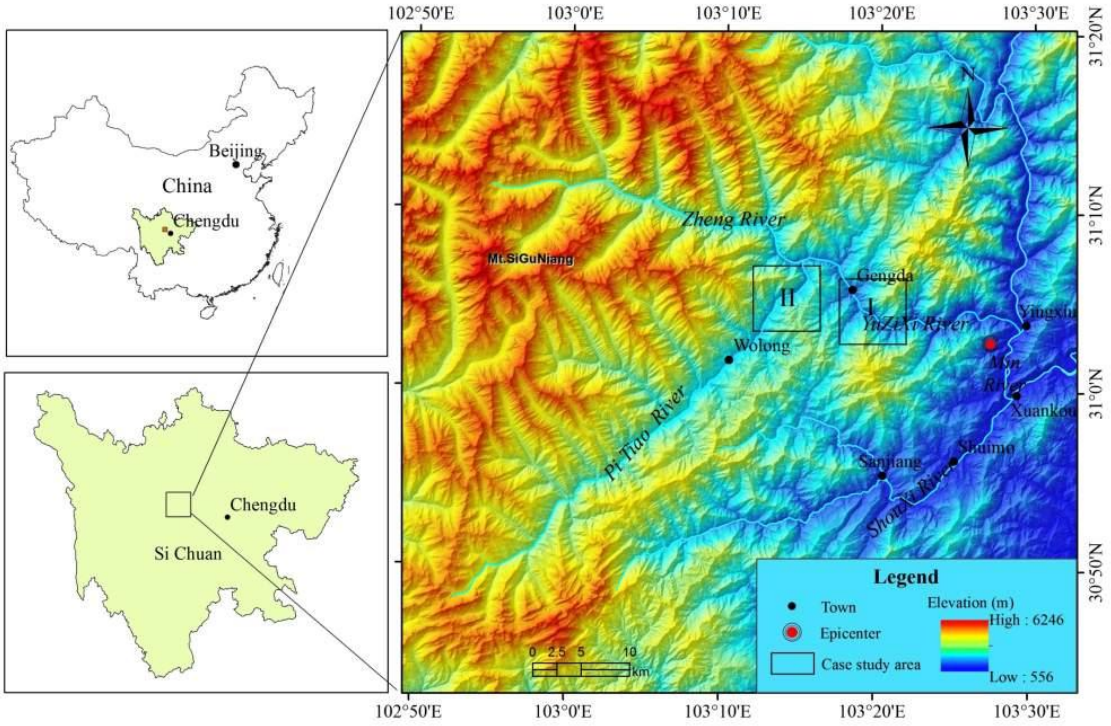


Fig. 2.2. Location map of the study area Yingxiu near the epicenter of the Wenchuan earthquake on 12 May 2008, and topographic features of a digital elevation model with 25 m resolution from the national topographic database of China.

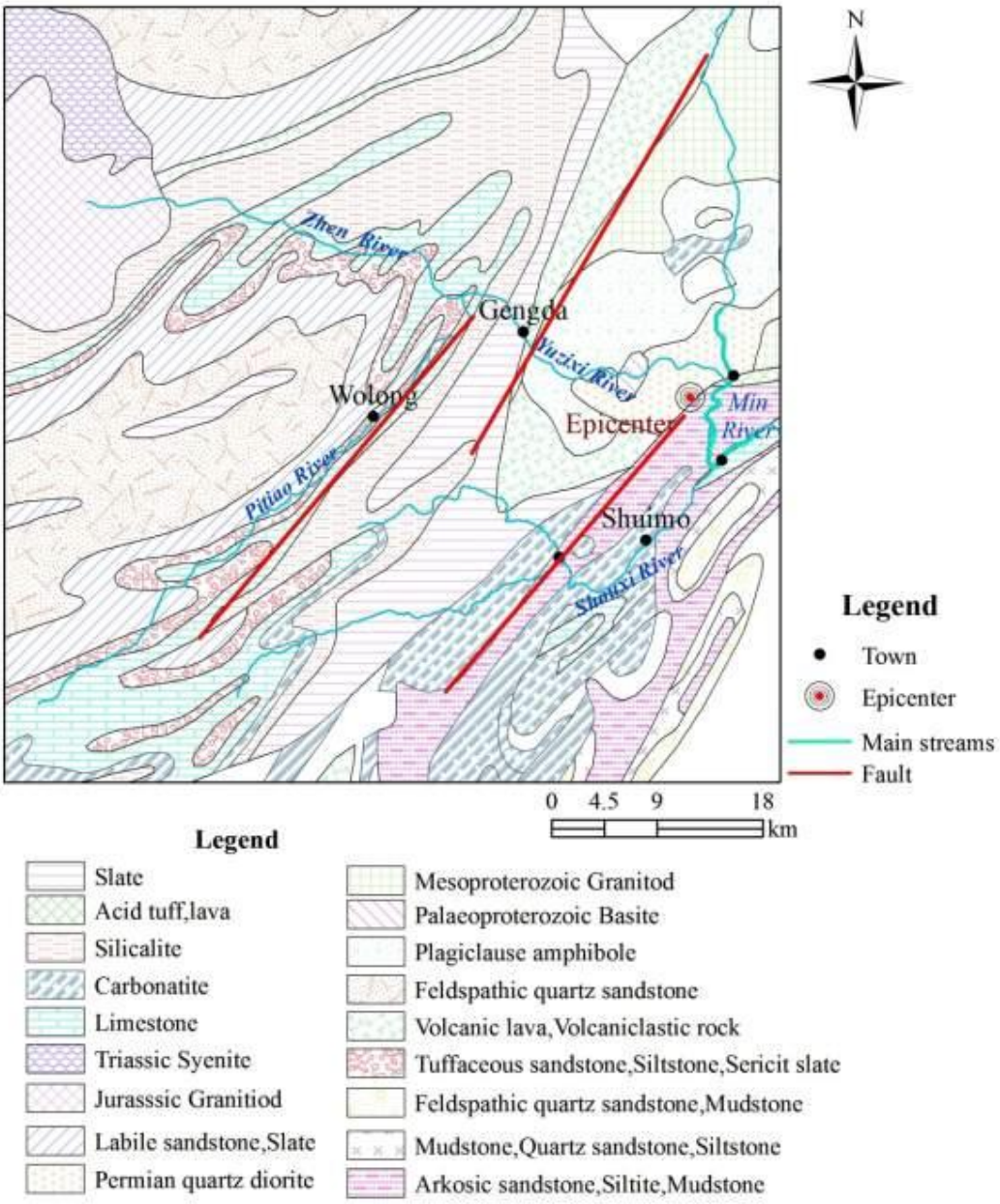


Fig. 2.3. Geological map of the study area produced by simplifying an original map by China Geological Survey (1996).

The surface geology of the study area is characterized by a zonal distribution of main rock types including Feld spathic quartz sandstone, labile sandstone, slate, silica lite and limestone (Fig. 2.3). These rocks are approximately divided chronologically into two

halves by the Pitiao River; the Paleozoic rocks exposed in the southeast side and the Triassic rocks in the northwest side. The eastern side of the study area around the epicenter is mainly overlain by carbonate, silicalite, volcaniclastic rock, plagioclase amphibole diorite and the Permian quartz diorite.

## 2.2 Methodology

### 2.2.1 Remote sensing

Just as its name implies, remote sensing involves the capture of images from some remote distance. Remote sensing can provide information on shape, color, position, temperature, moisture content, and the 'health' of vegetation (Wilkie and Finn, 1996).

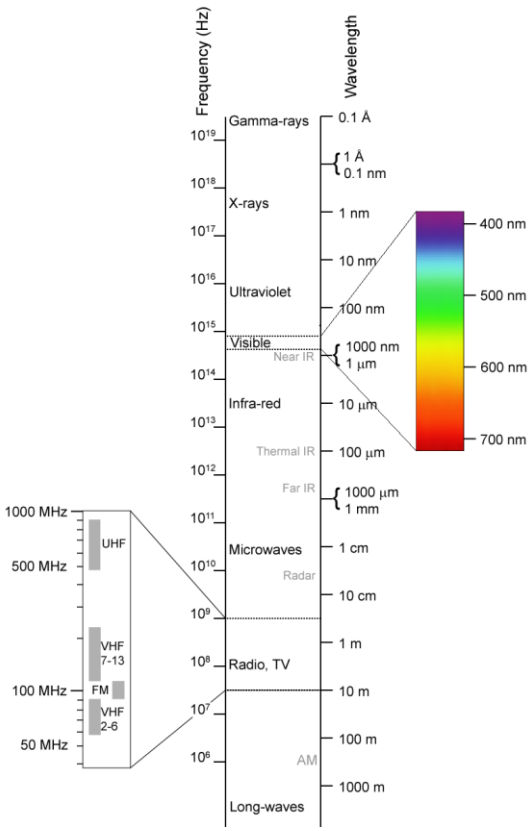


Fig. 2.4. The electromagnetic spectrum (image source: Wikipedia)

Most satellite remote sensing is based on detecting the way surfaces reflect and absorb visible and infrared radiation, a subset of the electromagnetic spectrum (Fig.2.4). The electromagnetic spectrum is a continuum of all electromagnetic waves arranged according to frequency and wavelength. The sun, earth, and other bodies radiate electromagnetic energy of varying wavelengths.

The percentage of incident light of particular wavelengths that is reflected by an object is referred to as spectral reflectance (the total quantity of energy reflected is termed radiance). Remote sensors detect the radiance associated with a given pixel and then this information is often converted to the spectral reflectance. Different cover types will each have their own spectral reflectance. For example, chlorophyll in vegetation primarily absorbs radiation in the blue and red wavelengths and reflects radiation in the green wavelengths. Thus, a pixel can be classified as deciduous forest, water, or barren soil, for example, based on its spectral reflectance.

Remote sensing and geographic information system techniques have been recently shown to be useful for environmental monitoring that aims to detect land cover change at various scales, estimate the temperature of the sea or ground surface, explore mineral resources, and monitor the activity of volcanoes (e.g., Wang *et al.*, 2009; Li *et al.*, 2008; Tian *et al.*, 2010; Stefanov, 2001; Wilson, 2003; Saepuloh *et al.*, 2010; Raharimahefa et al., 2010; Gabr et al., 2010).

### 2.2.2 Geographic Information Systems

A Geographical Information System (GIS) is a system of hardware, software and procedures to facilitate the management, manipulation, analysis, modeling, representation

and display of geo-referenced data to solve complex problems regarding planning and management of resources. Functions of GIS include data entry, data display, data management, information retrieval and analysis. The applications of GIS include mapping locations, quantities and densities, finding distances and mapping and monitoring change.

GIS are important tools for viewing broad-scale patterns of spatial data, organizing and integrating information about an area, and analyzing that data to answer questions. A GIS is more than a tool to make pretty maps. The basic GIS provide the user with the ability to store, manipulate, and display information about a region. What separates a GIS from a mere mapmaking program are the data, which are geographically referenced, can come from many sources, and can be manipulated and analyzed in a variety of ways.

### 2.2.3 Geostatistics

Geostatistics was developed by geologists to take into account variations of spatially correlated phenomena, such as the distribution of rocks or soils. Since landscape ecology relies largely on the existence of a mosaic made up of discrete entities with marked transitions, the use of geostatistics has not been well developed till recently. In addition, spatial dimension seldom having been taken into account in ecology, the geostatistics has not been integrated. Still, there are notable exceptional. For Example, Legendary and Fortin use geostatistics for spatial analysis within communities. They observe that the ecological data are often internally correlated that the value of a variable in a given place is dependent on or correlated to values of this variable in the neighborhood. This is linked to the existence of an environmental gradient, as well as to mechanisms of

dissemination of plant and animal organisms. Geostatistics are spatial statistics used to explore the correlativity and dependence between spatial variables based on regionalized variable theories (Journel and Huijbregts, 1978), which make it promising in ecology.

Semivariogram have been applied to quantify the spatial heterogeneity of landscape. Spatial heterogeneity is divided into two main parts: random variability and autocorrelation variability (Fig. 2.5). They are corresponding with small scale (e.g. resolution of remote sensing image) and middle scale respectively.

Semivariogram is created by measuring the distance between two locations and plotting the difference squared between the spatial values at the locations. On the x-axis is the distance between the locations, and on the y-axis is the difference of their values squared (Fig. 2.5). Each dot in the semivariogram represents a pair of locations.

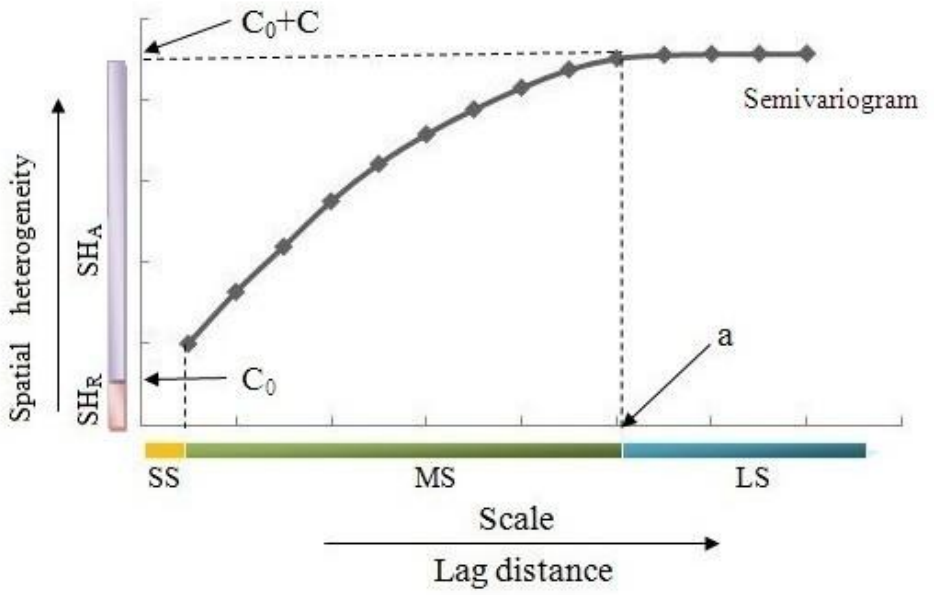


Fig. 2.5. Ecological meaning of semivariogram

If spatial correlation exists, pairs of points that are close together (on the far left of

the x-axis) should have less difference (be low on the y-axis). As points become farther away from each other (moving right on the x-axis), in general, the difference squared should be greater (moving up on the y-axis). Often there is a certain distance beyond which the squared difference levels out. Pairs of locations beyond this distance are considered to be uncorrelated.

Spatial autocorrelation may depend only on the distance between two locations, which is called isotropy. However, it is possible that the same autocorrelation value may occur at different distances when considering different directions. Another way to think of this is that things are more alike for longer distances in some directions than in other directions. This directional influence can be seen in semivariograms and is called anisotropy. If anisotropy exits in semivariogram within the image domain, it means that spatial variable appear to be the highest continuity along the direction of the major range.

### 2.2.4 Landscape ecology

Landscape ecology, as the name implies, is the study of landscapes; specifically, the composition, structure and function of landscapes. But what's a 'landscape'? Although there are myriad ways to define 'landscape' depending on the phenomenon under consideration, suffice it to say that a landscape is not necessarily defined by its size; rather, it is defined by an interacting mosaic of elements (e.g., ecosystems) relevant to some phenomenon under consideration (at any scale). Thus, a landscape is simply an area of land (at any scale) containing an interesting pattern that affects and is affected by an ecological process of interest. Landscape ecology, then, involves the study of these landscape patterns, the interactions among the elements of this pattern, and how these patterns and interactions

change over time. In addition, landscape ecology involves the application of these principles in the formulation and solving of real-world problems. Landscape ecology is perhaps best distinguished by its focus on: 1) spatial heterogeneity, 2) broader spatial extents than those traditionally studied in ecology, and 3) the role of humans in creating and affecting landscape patterns and process.

Landscape ecology might be defined best by its focus on spatial heterogeneity and pattern: how to characterize it, where it comes from, how it changes through time, why it matters, and how humans manage it. As such, landscape ecology has five central themes:

• Detecting pattern and the scale at which it is expressed, and summarizing it quantitatively.

• Identifying and describing the agents of pattern formation, which include the physical abiotic template, demographic responses to this template, and disturbance regimes overlaid on these.

• Characterizing the changes in pattern and process over space and time; that is, the dynamics of the landscape, and summarizing it quantitatively. An interest in landscape dynamics necessarily invokes models of some sort--because landscapes are large and they change over time scales that are difficult to embrace empirically.

• Understanding the ecological implications of pattern; that is, why it matters to populations, communities, and ecosystems – and this is the stuff of conservation biology and ecosystem management.

• Managing landscapes to achieve human objectives.

## 2. 3 Data Resource

Data comprised satellite images, topographic maps with a scale of 1:250,000, 25-m a digital elevation model (DEM) and ground observations. One image of advanced land observing satellite (ALOS) acquired on 1 February 2007 was used for classifying vegetation type. ALOS has three instruments of optical and microwave sensors: the panchromatic remote-sensing instrument for stereo mapping (PRISM) for digital elevation mapping, the advanced visible and near infrared radiometer type 2 (AVNIR-2) for precise land coverage observation, and the phased array type L-band synthetic aperture radar (PALSAR). We used AVNIR-2 image that provides high spatial resolution (10 m) maps of land-coverage land-use classification for monitoring regional environments by four band data that cover visible regions (0.42–0.50 μm, 0.52–0.60 μm and 0.61–0.69 μm) and the near-infrared region (0.76–0.89μm).

To detect vegetation change occurring before and after the earthquake, four scenes of Landsat-7 Enhanced Thematic Mapper (ETM+) data sets (Rows 38 and 39/Path 130 of WRS-2) acquired on 5 April 2008 and 23 May 2008 were used. The ETM+ sensor measures the Earth surface reflectance of electro-magnetic waves from the Sun's illumination at seven spectral bands: visible blue (0.45–0.52 μm), green (0.52–0.60 μm), red (0.63–0.69 μm), near-infrared (0.76–0.90 μm), short-wave infrared (1.55–1.75 and 2.08–2.35 μm), thermal infrared (10.5–12.5 μm) and panchromatic mode (0.52–0.90 μm).

## 2.4 Conclusion

This chapter aims at describing the study area in terms of the location, geology, and other environmental characters. Since the study area was selected around the epicenter of Wenchuan earthquake, some information about this earthquake was introduced as an available background for this research. Meanwhile, in this chapter, main methodologies utilized through this dissertation, remote sensing, geographic information systems, geostatistics and landscape ecology, were presented; e.g. their principles, advantages and relationship between each other. In this research, remote sensing, GIS and geostatistics are integrated to be a suitable method to achieve the objectives here. In the final part of this chapter, the data sources utilized in this dissertation were listed.

## References

China Geological Survey, 1996. Spatial database of 1:500,000 digital geological map of The People's Republic of China.

Wilkie, D. S., and J. T. Finn, 1996. Remote sensing imagery for natural resources monitoring: a guide for first-time users. Columbia University Press, New York.

Chigira, M., Wu, X., Inokuchi, T., Wang, G., 2010. Landslides induced by the 2008 Wenchuan earthquake, Sichuan, China. Geomorphology, 118: 225-238.

Davis, G., 1984. Structural Geology of Rocks and Regions, Wiley, New York, 475.

Fan, J., Chen, J., Tian, B., 2010. Rapid assessment of secondary disasters induced by the Wenchuan earthquake. Computing in Science & Engineering, 12(1):10-19.

Gabr S., Ghulam A., Kusky T., 2010. Detecting areas of high-potential gold mineralization using ASTER data. Ore Geology Reviews, 38(1-2):59-69.

Hara, M., Hirata, K., Fujihara, M., and Oono, K., 1996. Vegetation structure in relation to micro-landform in an evergreen broad-leaved forest on Amami Ohshima Island, Southwest Japan. Ecological Research, 11:325-337.

Huang, R., Li, W., 2008. Development and distribution of geohazards triggered by 5.12 Wenchuan earthquake in China. Science in China Series E: Technical Science, 52:810-819.

Journel, A. G., Huijbregts, C., 1978. Mining Geostatistics, Academic Press, San Diego, 600.

Li, X., Gu, B., Wang, L., 2008. The design of information system in hydropower development and its application in eco-environment research. Journal of Sichuan University (Nature Science Edition), 45(3): 687-693.

Masoud, A., Koike, K., 2006. Tectonic architecture through Landsat-7 ETM+/SRTM DEM-derived lineaments and relationship to hydrogeological setting in Siwa region, NW Egypt. Journal of African Earth Sciences, 45:467-477.

Ouimet, W., 2010. Landslides associated with the May 12, 2008 Wenchuan earthquake: Implications for the erosion and tectonic evolution of the Longmen Shan. Tectonophysics, 491:244–252.

Raharimahefa T., Kusky T.M., 2010. Environmental Monitoring of Bombetoka Bay and the Betsiboka Estuary, Madagascar, Using Multi-temporal Satellite Data. Journal of Earth Science, 21(2):210-226.

Ruland, W., Cherry, J., Feenstra, S., 1991. The depth of fractures and active ground-water flow in a clayey till plain in southwestern ontario. Ground Water, 29(3): 405-417.

Saepuloh, A., Koike, K., Omura, M., Iguchi, M., and Setiawan, A., 2010. SAR- and gravity change-based characterization of the distribution pattern of pyroclastic flow deposits at Mt. Merapi during the past 10 years. Bull.Volcano., 72:221–232.

Tang, H., Jia, H., Hu, X., Li, D., Xiong, C., 2010. Characteristics of landslides induced by the great Wenchuan earthquake. Journal of Earth Science, 21: 104-113.

Tian, B., Wang, L., Koike, K., Fan, J., 2010. Analysis and assessment of earthquake-induced secondary mountain disaster chains based on multi-platform remote sensing. 2010 IEEE International Geosciences and Remote Sensing Symposium Proceedings, Honolulu, Hawaii, USA, July 25-31,1214-1217. (doi: 10.1109/IGARSS.2010.5648963).

Tucker, C. J., 1979. Red and photographic infrared linear combinations for monitoring vegetation. Remote Sensing of Environment, 8(2):127-150.

Wang, L., Gu, B., Tian, B., 2009. Dynamically monitoring of Minjiang area based on RS data—a case of Wenchuan County. Journal of Sichuan University (Nature Science Edition), 46(3): 803-808.

Wilson, E., Hurd, J., Civco, D., et al., 2003. Development of a geospatial model to quantify, describe and map urban growth. Remote Sensing of Environment, 86: 275-285.

# Chapter 3

# Characteristic of Fracture Zones and Vegetation Change

## 3. 1 Introduction

Fracture zones on the earth's surface are important elements in the understanding of plate motion forces, the dynamics of the subsurface fluid flow, and earthquake distributions. The Wenchuan earthquake and its strong aftershocks activated Longmenshan fracture system that marks the transition between mountains of the Tibetan Plateau and the Sichuan Basin. It is thought that the earthquake occurred as a result of long-term uplift and eastward extrusion of the Tibetan Plateau. The active Longmenshan fracture system comprises the NE-SW-striking Wenchuan-Maoxian Fault in the northwest, the Yinxiu-Beichuan Fault in the central portion and the Guanxian-Anxian Fault in the southeast, of which the Yinxiu-Beichuan Fault is inferred to be the main structure that generated the Whenchuan earthquake. Most research has focused on the landslides triggered by the Wenchuan earthquake to identify their distributions; the landslides were mostly concentrated in two areas, near the seismogenic fault and on the steep slopes adjacent to the Minjiang River (Huang et al., 2008; Chigira et al., 2010; Tang et al., 2010; Fan et al., 2010). Landslide is one of the most important events causing vegetation pattern change after a large earthquake because it converts vegetation cover into bare area. Monitoring vegetation change by comparing satellite images before and after an earthquake has been widely used to detect the location and extent of landslides (e.g., Fan et al., 2010; Ouimet, 2009). However, except for several representative active faults such as the Longmenshan fracture zones, the regional changes of vegetation pattern induced by an earthquake and their relationships with fracture zones have not been examined in detail.

Fracture zones can be viewed at a large geographic scale on satellite images and

aerial photographs in the form of lineaments as simple, composite-pattern linear or curvilinear features discernible on the Earth's surface. Remote sensed linear features, largely a reflection of rock fractures, emphasized by vegetation and topography, has been evidenced by successful use of lineament analysis in exploration of oil and gas traps, and to select drilling locations for maximum porosity in tight formations. Lineaments originate mainly from strains that arise from stress concentrations around flaws and physical discontinuities (O'Learly et al., 1976; Davis, 1984; Clark and Wilson, 1994). They form in response to lithostatic, tectonic, and thermal stresses and high fluid pressures.

In this chapter, a segment tracing algorithm method (Koike et al., 1995; 1998) is applied to extract lineaments and then to identify the orientation, continuities, densities, and intersecting patterns of the fracture zones. In addition, earthquake induced vegetation change pattern was analyzed associated with fracture zone to find out relationships between them.

## 3.2 Method

### 3.2.1 Lineament extraction

Conventional lineament extraction techniques, commonly based on visual interpretation and hand-tracing of linear features depicted on aerial photographs or paper-based satellite image mosaics, are time-consuming, tedious, subjective and irreproducible. As for auto-extraction of lineament, the approaches are generally based on edge enhancement and filtering techniques, which produce short dense lineaments that are difficult to relate to tectonically significant structures. Additionally, extraction and characterization of fracture zones are difficult in most cases because they are generally

concealed by thick surficial sediments (Masoud and Koike, 2006). Traditional extraction techniques of lineaments from satellite images are limited in both the amount and distribution. To overcome this problem, Koike et al. (1995; 1998) proposed a non-filtering technique, the segment tracing algorithm (STA), which has the advantage of (1) tracing only continuous valleys and (2) extracting more lineaments that are parallel to the sun's azimuth as well as those located in shadow areas.

The procedure of the STA is to first define a line that is composed of adjacent pixels as a vector element by examining local variance of reflectance along their expected directions. Then, to avoid solar illumination bias and to select tectonically significant lineaments, flexible and directional dependent thresholds are adopted for both the extraction and linkage of the line elements.

### 3.2.2 Vegetation change using NDVI

To detect vegetation change occurring before and after the earthquake, four scenes of Landsat-7 enhanced thematic mapper (ETM+) data sets (Rows 38 and 39/Path 130 of WRS-2) acquired on 5 April 2008 and 23 May 2008 were used. These remote sensing images were first orthorectified based on the available raster DEM and then geo-referenced to the UTM coordinate system Zone 48 North with other related data. Two adjacent scenes of the geo-referenced ETM+ images for each time were merged to one scene and clipped to the study area.

Normalized difference vegetation index (NDVI), which has been demonstrated to be a useful indicator of overall green biomass, canopy closure, tree density, and tree species diversity, has the formula:

$$NDVI = \frac{R_{NIR} - R_{RED}}{R_{NIR} + R_{RED}} \quad (1)$$

Where $R_{RED}$ and $R_{NIR}$ are the reflectance at visible red and near-infrared bands, respectively (Tucker, 1979). Higher NDVI signifies a greater level of photosynthetic activity (Sellers, 1985). The value of NDVI ranges from -1 to 1 with negative values corresponding to non-vegetated surfaces and positive values corresponding to vegetated ones.

Although NDVI is sensitive to soil and atmospheric effects, it is a good indicator of the vegetation amount (Henebry, 1993). Moreover, the topographic effect on the NDVI can usually be ignored (Matsushita, 2007), which makes it more valuable in studies of mountainous areas. Significant differences in NDVI values before and after a natural disturbance, such as a large earthquake as under investigation in the present study, can correctly represent landscape changes from plant-covered land to bare land or from bare land to plant-covered land (Lin, 2006).

The destruction of vegetation caused by the Wenchuan earthquake was revealed from change of NDVI values of ETM+ images before and after the earthquake. Areas at which the NDVI after the earthquake minus that before was smaller than zero were defined as the destroyed areas. Because the vegetation is greener in May than in April, the change of NDVI values must be larger than zero according to this definition. Therefore, minus values of NDVI change suggests abnormal vegetation growth induced by the earthquake.

## 3.3 Characterization of fracture zones

For the lineament extraction, a shaded image was produced from the DEM data at a 25 m interval following the method proposed by Masoud and Koike (2011), which is an adaptive tilt multi-directional shading technique. This technique assigns the maximum shade intensity by changing illumination azimuth and dip to the kernel center of a small window in the DEM. Such a shaded DEM image can highlight topographical features more clearly than a satellite image by excluding the Sun's illumination effect and artificial linear pattern of reflectance related to the boundary of surface materials. By field checks, most lineaments extracted from the shaded DEM image by STA were found to correspond with the conspicuous topographic discontinuities composed of faults, rivers and valleys, which were generally related to regional fracture systems (Masoud and Koike, 2011 a & b). A total number of 109,048 lineaments were extracted by STA from the shaded DEM image with lengths ranging from 0.03 to 6.34 km (Fig. 3.1 A).

The lineaments were then grouped into longer fracture zones according to similarity of direction and nearness of location following the method of Koike et al. (1998). Fig. 3.2 shows the polar plot of the finally grouped fracture planes represented by azimuthal length and azimuthal frequencies of the strike and dip of the planes, using the lower hemisphere projection of the Schmidt net. It is clear from the resultant lineament map (Fig. 3.1B) and Fig 3.2 that the majority of lineaments strike NE-SW with few long lineaments oriented NW-SE, commonly in the northwestern side of Pitiao River.

Next, a lineament density map was produced to characterize the heterogeneity of lineament distribution by counting the number of centers of lineaments per $km^2$ (Fig. 3.3). The high lineament density zones tend to be distributed along a northeast direction. Three

major fracture zones were detected from the dense zones of the interpreted fractures, which corresponded with Pitiaohe, Gengda and Yingxiu Faults from northwest to southeast, by referring to a geological structure map of Sichuan province and literature from state forestry administration, R.R. China. The strikes of these three fracture zones are N30-50°E.

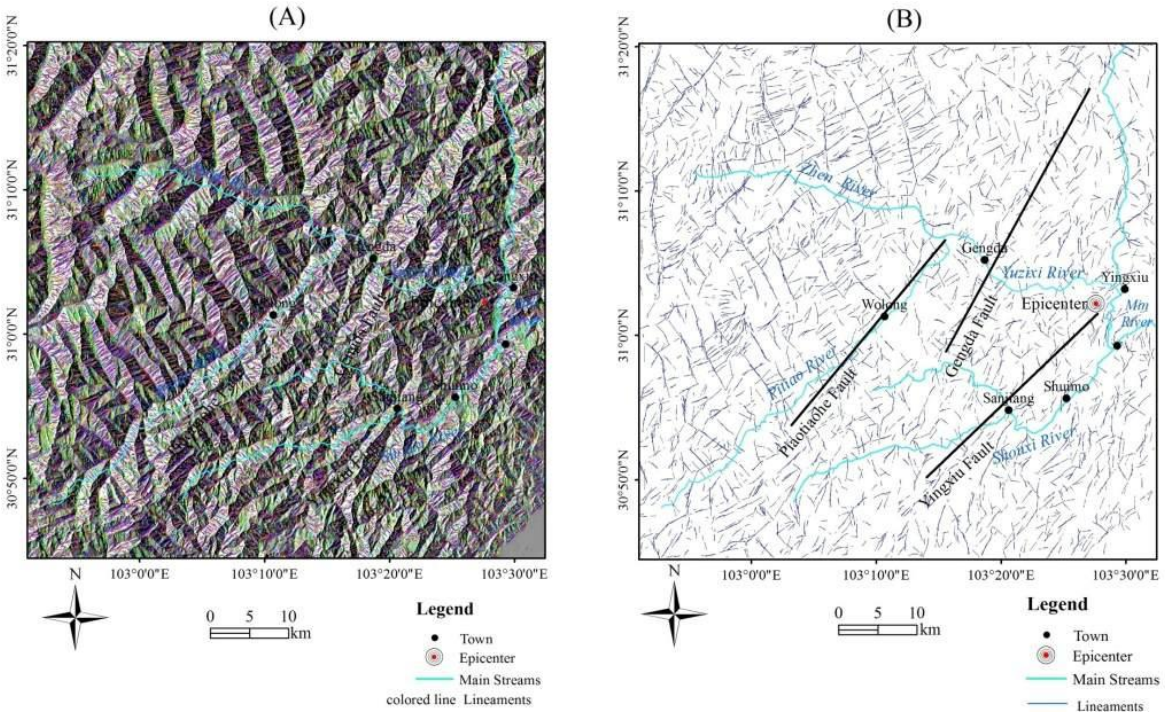


Fig. 3.1. Lineaments extracted through a segment tracing algorithm from a shaded digital elevation model (DEM) image. (A) Lineaments superimposed on DEM. Different line colors represent different direction and length of lineaments. Purple and blue lines represent long lineaments with directions of around N45°E, and green and yellow lines represent short lineaments with directions of around N45°W. (B) Grouped lineaments according to similarity of direction and nearness of location. Three black lines represent faults.

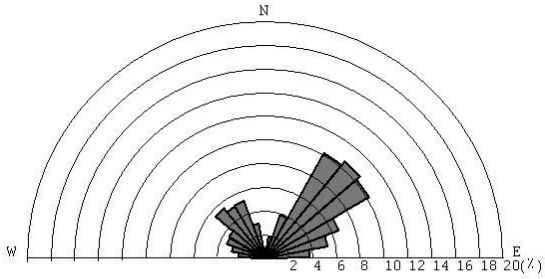


Rose diagram

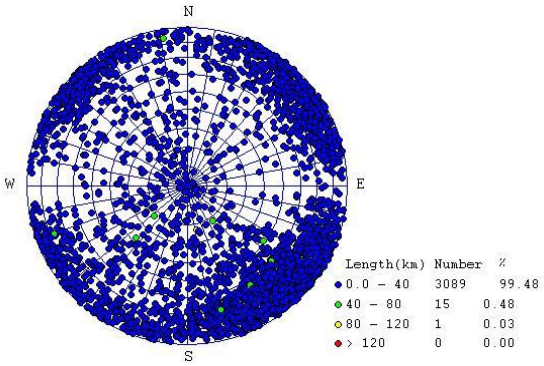


Azimuthal length

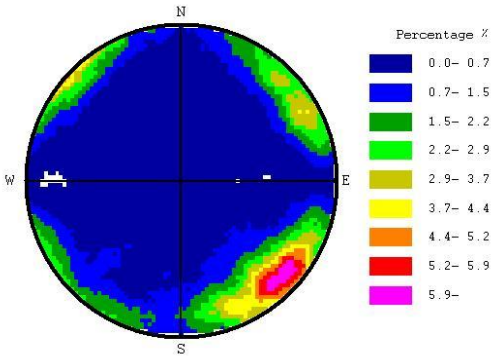


Azimuthal frequency

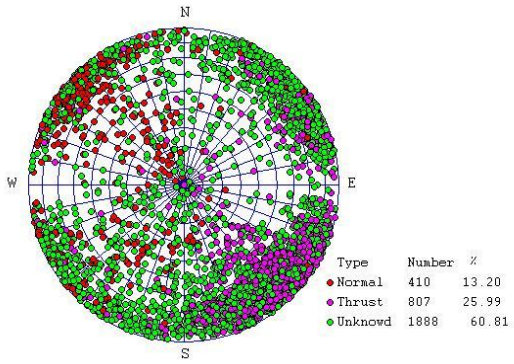


Fault type

Fig. 3.2. Rose, azimuthal length, azimuthal frequency and Fault type diagrams of lineament identified by STA.

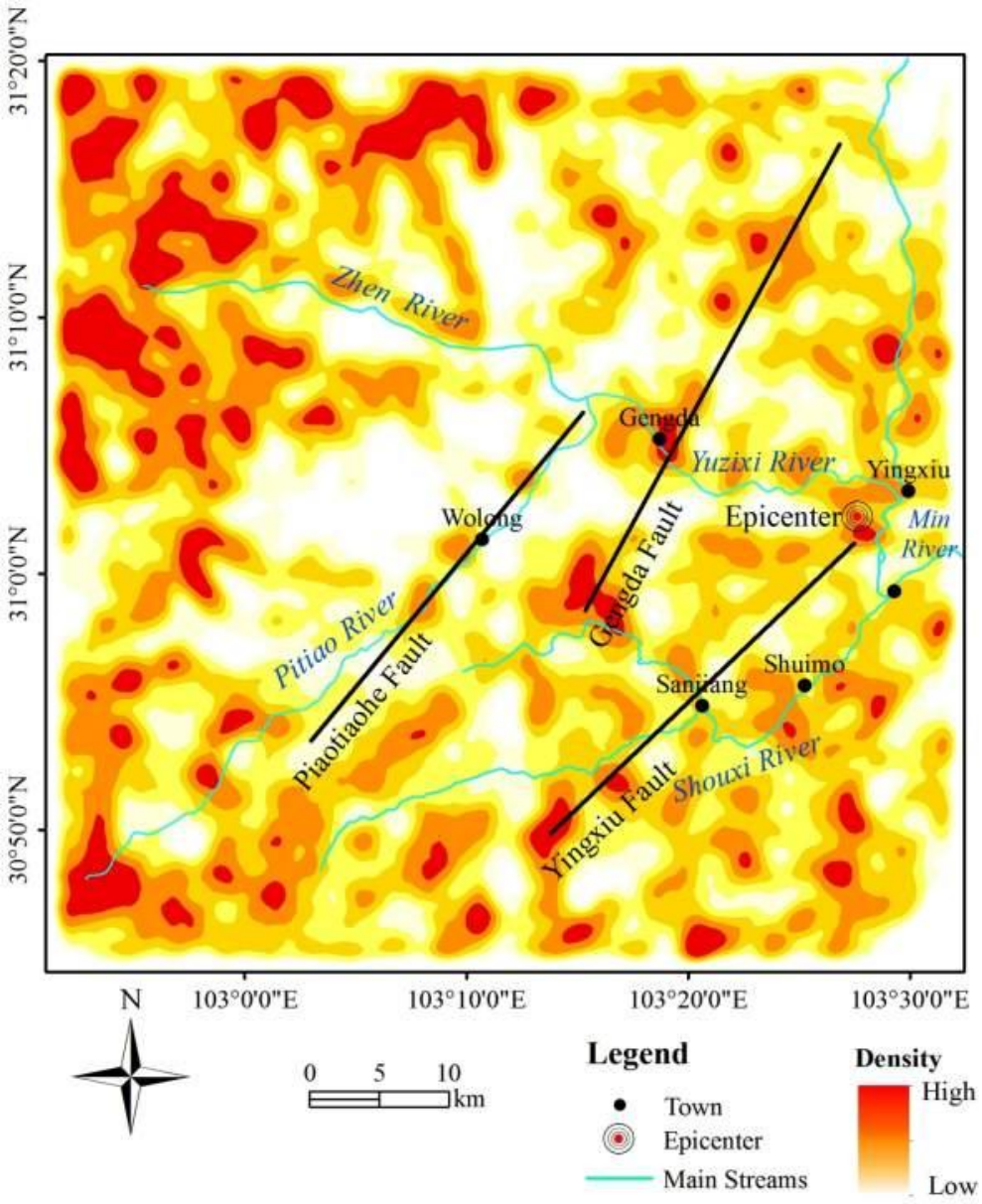


Fig. 3.3. Lineament density map for characterizing the heterogeneity of lineament distribution by counting the number of centers of lineaments per unit area. Three faults, shown as solid black lines, are superimposed on the density map.

## 3.4 Relationship between vegetation change and fracture zones

The destruction of vegetation caused by the Wenchuan earthquake was revealed from change of NDVI values of ETM+ images before and after the earthquake. Areas at which the NDVI after the earthquake minus that before was smaller than zero were defined as the destroyed areas. Because the vegetation is greener in May than in April, the change of NDVI values must be larger than zero according to this definition. Therefore, minus values of NDVI change suggests abnormal vegetation growth induced by the earthquake.

The destroyed areas are shown in Fig. 3.4. By comparing their distribution with the lineament density map (Fig. 3.3), it is conspicuous that these areas are generally consistent with the fracture zones. The most severely destroyed areas were concentrated around the epicenter. The areas that were less destroyed lie at the intersection of Pitiao and Zheng Rivers around Pitiaohe Fault. However, vegetation in the western part of the study area was only a little or not destroyed even though it was located in the highest lineament density zones. The western part of the study area was mainly covered by hard rocks such as silicalite, limestone, and slate (Fig. 2.3) and, therefore, it was relatively stable despite the earthquake. Another influential factor for the degree of vegetation damage was elevation. Elevations generally decreased eastwardly towards the epicenter (see Fig. 2.2) and the damage became more severe along this direction, which suggests that higher elevation areas were less affected by the earthquake.

Softer rocks such as quartz diorite and amphibole diorite were dominant in the eastern part of the study area, which contributed to the severity of the damage. The severe damage spread about 15 km westwards from the epicenter and sharply diminished mostly at Gengda Fault. Therefore, Gengda Fault may have reduced the earthquake power by

acting as a shield and focused the seismic energy northward, as suggested by Kusky et al. (2010).

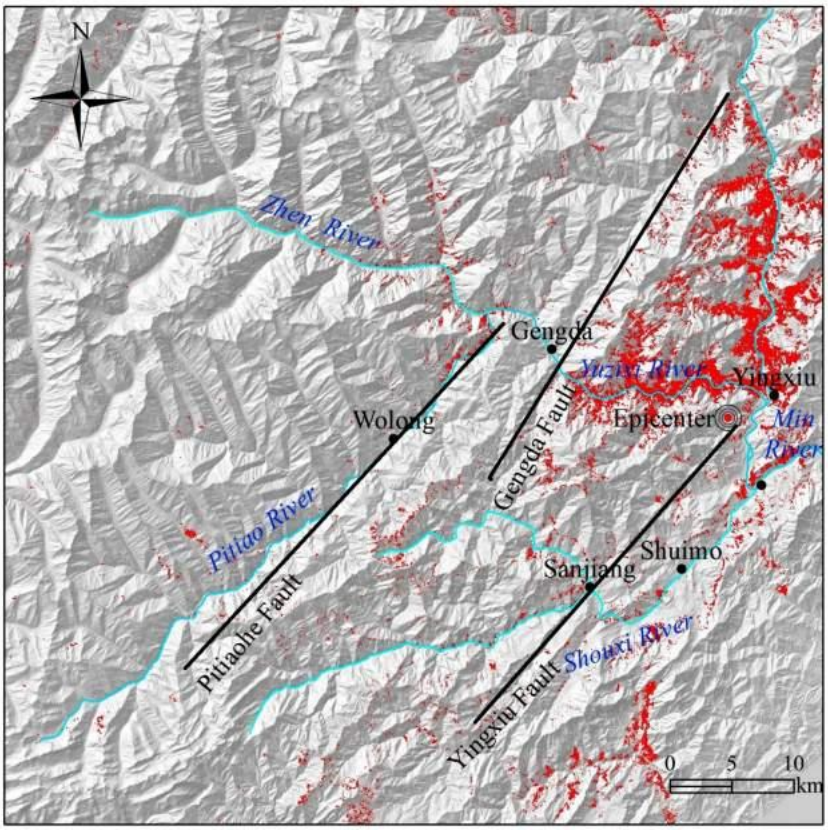


Fig. 3.4. Destroyed vegetation areas (red) detected by a decrease of NDVI values in the Landsat ETM+ image after the Wenchuan earthquake.

Figure 3.4 presents another characteristic of the vegetation destruction according to the positional relationship with rivers. The vegetation areas were destroyed much more severely in the Yuzixi watershed than in the Shouxi basin. Three faults all passed through the domain of Yuzixi watershed, while only one fault, Yinxiu Fault, was situated in the Shouxi basin. There were two accordant junctions in the Yuzixi watershed. The severely destroyed vegetation was located in the accordant junction of Yuzixi River flowing to Min

River, by the epicenter and Yingxiu Fault. The damage in the accordant junction of Zhen River descending to Yuzixi River was less severe than in the other accordant junction, but relatively heavier compared with that of the whole study area. The damage in this area associated with Pitiaohe Fault, which was far from the epicenter, indicates that less earthquake energy was received in this area.

Additionally, the area suffered from vegetation change that was correlated with graded lineament density (Fig.3.5). The vertical axis shows the proportion of such area out of the total area for each lineament density level. Clearly, the magnitude of vegetation change increased with increasing lineament density, with a maximum at lineament density level 7. Thus, this confirms that the effect of the degree of fracturing on vegetation change was strong. One interpretation of this relationship is that the hydraulic conductivity in the highly fractured zone was greater, allowing water to flow rapidly in the unsaturated and saturated zones. Accordingly, groundwater level change followed the earthquake, which may have strongly affected the vegetation in the zone.

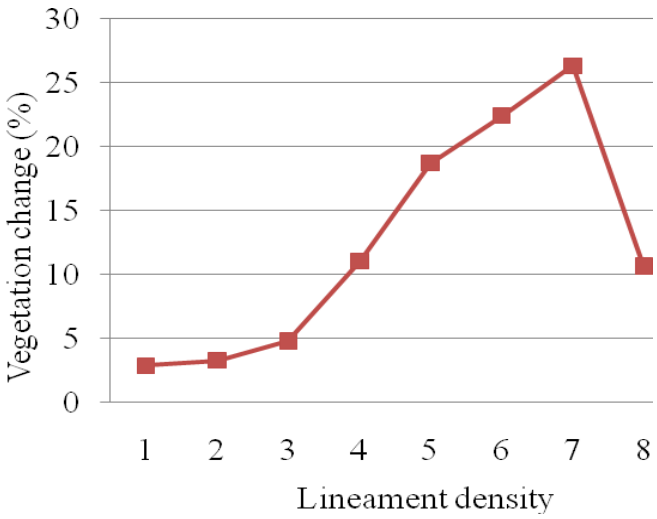

Fig. 3.5. Relationship between the areas suffering from vegetation change and the graded lineament density. The vertical axis shows the proportion of such area out of the total area for each lineament density level.

## 3.5 Conclusion

An effective algorithm for segment tracing of lineaments has been applied in the study area. Three major fracture zones trending NE-SW were detected. The destructed vegetations were generally consistent with the fracture zones. Moreover, the distribution of the ruined areas corresponds with the accordant junction of the watersheds. The elevation and distance from the epicenter may be important factors controlling the distribution of the destructed areas of the vegetation induced by the earthquake.

The distributions of the areas suffering from severe vegetation destruction were generally consistent with those of the fracture zones. The most severely damaged areas were located around the epicenter and spread toward the west and northwest to Gengda Fault. This fault may have functioned as a shield weakening the earthquake energy. The less severely destroyed areas lied around Pitiaohe Fault, located to the west of Gengda Fault. This fault was relatively far from the epicenter and this indicates that less earthquake energy was received in this area.

## References

Clark, C., Wilson, C., 1994. Spatial analysis of lineaments. Computers and Geosciences, 20:1237-1258.

Chigira, M., Wu, X., Inokuchi, T., Wang, G., 2010. Landslides induced by the 2008 Wenchuan earthquake, Sichuan, China. Geomorphology, 118: 225-238.

Davis, G., 1984. Structural Geology of Rocks and Regions, Wiley, New York, 475.

Gao, Z., Liu, J., 2000. The study on driving factors and models of NDVI change based on remote sensing and GIS in China. Climatic and Environmental Research, 5(2):155-164.

Fan, J., Chen, J., Tian, B., 2010. Rapid assessment of secondary disasters induced by the Wenchuan earthquake. Computing in Science & Engineering, 12(1):10-19.

Hara, M., Hirata, K., Fujihara, M., and Oono, K., 1996. Vegetation structure in relation to micro-landform in an evergreen broad-leaved forest on Amami Ohshima Island, Southwest Japan. Ecological Research, 11:325-337.

Henebry, G., 1993. Detecting change in grasslands using measures of spatial dependence with Landsat TM. Remote Sensing of Environment, 46: 233-234.

Huang, R., Li, W., 2008. Development and distribution of geohazards triggered by 5.12 Wenchuan earthquake in China. Science in China Series E: Technical Science, 52:810-819.

Koike, K., Nagano, S., Ohmi, M., 1995. Lineament analysis of satellite images using a Segment Tracing Algorithm (STA). Computers and Geosciences, 21(9):1091-1104.

Koike, K., Nagano, S., Kawaba, K., 1998. Construction and analysis of interpreted fracture planes through combination of satellite-image derived lineaments and digital elevation model data. Computers and Geosciences, 24(6):573-583.

Kusky, T.M, Ghulam, A., Wang, L., Liu, J.G., Li, Z.Q., Chen, X.A., 2010. Focusing seismic energy along faults through time-variable rupture modes: Wenchuan earthquake, China. Journal of Earth Science, 21(6):910-922.

Lin, W., Lin, C., Chou, W., 2006. Assessment of vegetation recovery and soil erosion at landslides caused by a catastrophic earthquake: a case study in central Taiwan. Ecol. Eng., 28:79-89.

Masoud, A., Koike, K., 2006. Tectonic architecture through Landsat-7 ETM+/SRTM DEM-derived lineaments and relationship to hydrogeologic setting in Siwa region, NW Egypt. Journal of African Earth Sciences, 45:467-477.

Masoud, A., Koike, K., (2011a). Morphotectonics inferred from the analysis of topographic lineaments auto-detected from DEMs: application and validation for the Sinai Peninsula, Egypt. Tectonophysics (in press, doi:10.1016/j.tecto.2011.07.010).

Masoud, A., Koike, K., (2011 b). Auto-detection and integration of tectonically significant lineaments from SRTM DEM and remotely-sensed geophysical data. ISPRS Journal of Photogrammetry and Remote Sensing (in press, doi:10.1016/j.isprsjprs.2011.08.003).

Matsushita, B., Yang, W., Chen, J., 2007. Sensitivity of the Enhanced Vegetation Index (EVI) and Normalized Difference Vegetation Index (NDVI) to topographic effect: A case study in high-density cypress forest. Sensors, 7:2636-2651.

O'Learly, D., Friedman, J., Pohn, H., 1976. Lineament, linear, lineation: some proposed new standards for old terms, Bulletin of the Geological Society of America, 87:1463-1469.

Ouimet, W., 2010. Landslides associated with the May 12, 2008 Wenchuan earthquake: Implications for the erosion and tectonic evolution of the Longmen Shan. Tectonophysics, 491:244–252.

Ruland, W., Cherry, J., Feenstra, S., 1991. The depth of fractures and active ground-water flow in a clayey till plain in southwestern ontario. Ground Water, 29(3): 405-417.

Sellers, P., 1985. Canopy reflectance, photosynthesis and transpiration. Int. J. Remote Sens., 6: 1335–1372.

Stefanov, W., Ramsey, M., Christensen, P., 2001. Monitoring urban land cover change: an expert system approach to land cover classification of semiarid to arid urban center. Remote Sensing of Environment, 77: 173-185.

Tang, H., Jia, H., Hu, X., Li, D., Xiong, C., 2010. Characteristics of landslides induced by the great Wenchuan earthquake. Journal of Earth Science, 21: 104-113.

Tucker, C. J., 1979. Red and photographic infrared linear combinations for monitoring vegetation. Remote Sensing of Environment, 8(2):127-150.

Wang, L., Koike, K., Masoud, A., 2011. Relationship between remotely-sensed vegetation change and fracture zones induced by the 2008 Whenchuan Earthquake, China Journal of Earth Science (Springer: under second review).

Wang, L., Koike, K., Masoud, A., 2009. Characterization of fracture distributions and vegetation changes around the 2008 Sichuan earthquake epicenter (China) by satellite remote sensing. Proceeding of International Symposium on Earth Science and Technology, Fukuoka, December 8-9, 2009, pp. 387-390.

Wilson, E., Hurd, J., Civco, D., et al., 2003. Development of a geospatial model to quantify, describe and map urban growth. Remote Sensing of Environment, 86: 275-285.

# Chapter 4

# Relationship between Vegetation Type and Fracture Zones

## 4. 1 Introduction

Vegetation distribution is determined by diverse environmental conditions at different spatial scales. At regional and global scales there is predictability of certain vegetation characteristics, especially physiognomic ones, which are related to the predictability in certain environmental characteristics. Much of the variation in these global patterns is directly explainable by corresponding patterns of temperature and precipitation (sometimes referred to as the energy and moisture balances). These two factors are highly interactive in their effect on plant growth, and their relationship to each other throughout the year is critical. At such scale, vegetation pattern is dependent on solar radiation, climate and temperature (Qu et al., 1984; Gao et al., 2000). At a local scale, small scale, topography becomes a dominant factor controlling vegetation distribution because it can reallocate locally water and solar radiation (Hara et al., 1996).

However, fracture zones including faults, gouges and continuous joints can influence the vegetation pattern more strongly than topography by changing hydraulic conductivity and other soil properties around the fracture zone. In particular, vegetation patterns such as alignment of the same vegetation type may be formed by fracture zones that control groundwater flow (Ruland et al., 1991) and produce various soil types by strong weathering processes. Accordingly, the distribution of vegetation is expected to correlate with the fracture zone. Despite its importance, few studies have focused on furthering understanding of this relationship.

## 4.2 Data resource and processing

Data utilized in this chapter comprised four scenes of Landsat TM images dated on 25 July 2006 and 18 September 2007, with path 130 and row 38 and 39, and one image of advanced land observing satellite (ALOS) acquired on 1 February 2007.

### 4.2.1 Vegetation cover

ALOS was used for classifying vegetation type. A hybrid unsupervised-supervised approach of image classification (Brown, 1994) was applied to the ALOS image data to characterize the main vegetation types of the study area. This approach is a combination of two procedures, ISODATA (Iterative Self-Organizing Data Analysis Technique) and maximum-likelihood. Fifteen spectral clusters were identified using the ISODATA. All image pixels were then classified into one of the clusters using maximum-likelihood. Several clusters were identified to be one vegetation type through interactive interpretation. Classes were defined to match seven categories of the main vegetation types in the study area: evergreen broad-leaved forest; deciduous broad-leaved forest; deciduous and evergreen broad-leaved forest; coniferous forest; meadow; farmland; shrub and the other class, such as snow, ice, and water body, which was unrelated to vegetation. The accuracy of the resultant vegetation classification map was assessed by comparison with pictures with GPS position information and WorldView-1 imagery of 0.5 m resolution. High accuracy of the classification was also confirmed by largeness of the average of Kappa coefficient, 0.89 for all the classes.

### 4.2.2 Geostatistical techniques

Geostatistical techniques were employed to investigate the relationship between fracture zones and vegetation patterns. Geostatistics are spatial statistics used to explore the correlativity and dependence between spatial variables based on regionalized variable theories (Journel and Huijbregts, 1978). It includes two techniques: semivariograms, which model spatial dependence, and kriging, which provides estimates for unsampled locations. Garrigues (2006) reviewed several spatial tools, such as local variance, fractal, spatial entropy, semivariogram, Fourier transform and wavelet transform, which can characterize spatial heterogeneity of landscape vegetation cover, and concluded that NDVI semivariograms were most appropriate for this purpose. A fundamental assumption of geostatistics is that any two sample locations that are separated by a similar distance and direction should have a similar difference squared of data values. This relationship is called stationarity.

In this paper, NDVI data were considered as a regionalized variable z(x). At first, the experimental semivariogram γ(h) was computed at the NDVI image domain, which measures the average of the squared differences between values $z(x_\alpha)$ and $z(x_\beta)$ of paired pixels ($x_\alpha$, $x_\beta$) separated by vector h.

$$\gamma(\mathbf{h}) = \frac{1}{2N(\mathbf{h})} \sum_{\|\mathbf{x}_\alpha - \mathbf{x}_\beta\| = \mathbf{h}} \{z(\mathbf{x}_\alpha) - z(\mathbf{x}_\beta)\}^2 \quad (1)$$

If a spatial correlation exists, pairs of points that are closer together should have more similar values. At a large distance, it may reach a sill that is an indicator of the spatial variability of the data. The range is the distance at which γ(h) reaches the sill. Pairs of locations beyond the range are considered to be uncorrelated. A discontinuity of the γ(h) at

the origin, termed the nugget effect, can be caused by either uncorrelated noise (measurement error) or nested spatial structures at a scale smaller than that of the pixel size.

Spatial autocorrelation that depends only on the distance between two locations is called isotropy, while directional influence in $\gamma(h)$ which yields different autocorrelation values at the same distance depending on direction is called anisotropy. If anisotropy exits in NDVI $\gamma(h)$, vegetation pattern is bound to be the highest continuity along the direction of the major range. Therefore, the NDVI $\gamma(h)$ is capable of characterizing vegetation pattern.

## 4.3 Relationship between vegetation type and lineament

### 4.3.1 NDVI and Faults

NDVI provides a standardized method of comparing vegetation greenness between satellite images and effectively discriminates areas with healthy green vegetation from areas with soil/rocks. High NDVI values indicate intense photosynthetic activity of green vegetation. Many researchers even used NDVI to discriminate different vegetation types. Because NDVI is a good indicator to vegetation, here, initially, we took account into it to roughly check its relationship to lineament.

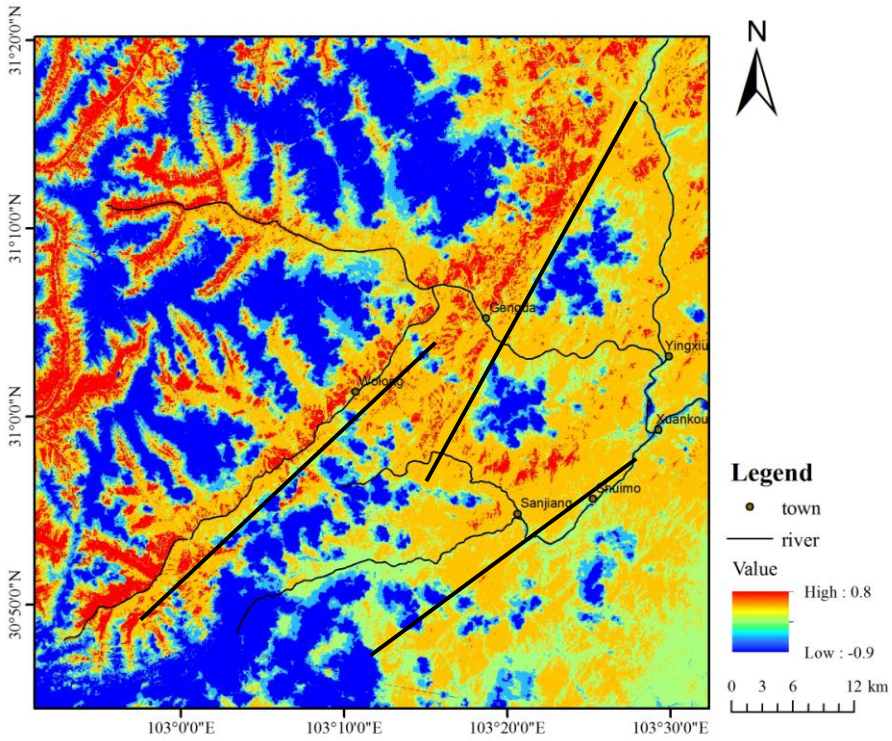


Fig. 4.1. NDVI calculated from Landsat TM images on 20060725

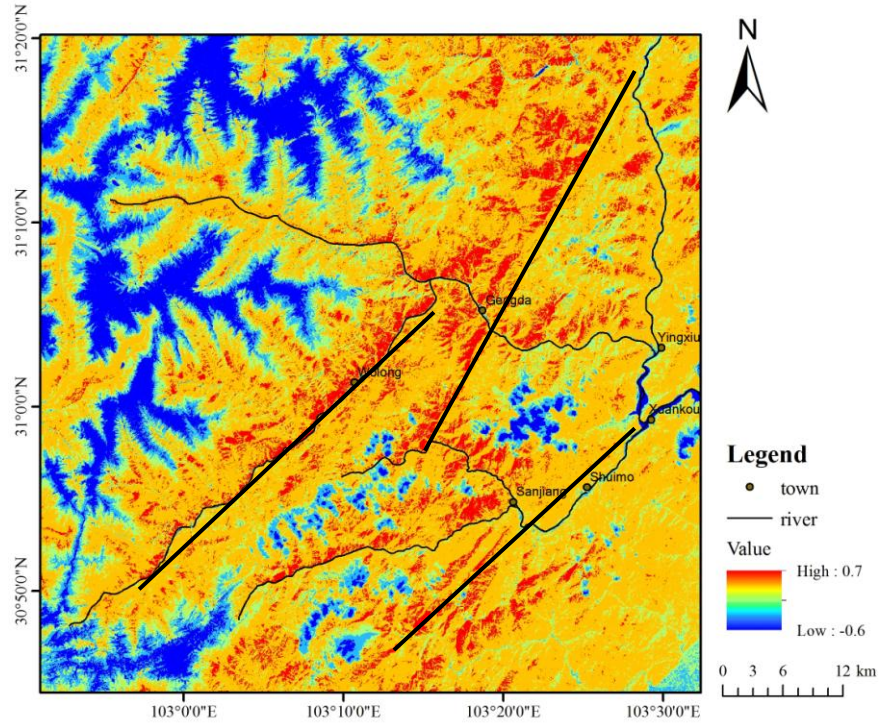


Fig. 4.2. NDVI calculated from Landsat TM images on 20070918

Two dates of Landsat TM images, 25 July 2006 and 18 September 2007, were selected to calculate the NDVI. Both were in the periods when all types of vegetation were flourished thrived.

Three main faults identified from STA, Pitiaohe Fault, Gengda Fault and Yingxiu Fault were overlaid on the both NDVI images. Coincidently, both Fig.4.1 and Fig.4.2 have same characteristics; one is that in either side of the faults, especially Pitiao Fault and Gengda Fault, the values of NDVI are quite different but have the same trend along the faults. In the left side of Pitiao Fault and Gengda Fault, NDVI appear high value than that in the right side of the faults. Such Characteristic is more obvious in NDVI on 18 September. One reason could be that vegetation in this time is growing well and exhibit more diversity than that on 25 July. The characteristics presented before indicate that vegetation cover types along different side of faults might be different.

### 4.3.2 Vegetation covers type and lineament

To characterize the relationship between vegetation cover types and fracture zone, the study area was classified into the seven vegetation types previously stated as shown in Fig. 4.3 It is clear from this figure that the study area mostly comprised forests, which were predominately coniferous forest.

Three major fracture zones were overlaid on the vegetation classification map to examine the vegetation types around the fracture zones. In the case of Pitiaohe Fault, the vegetation types were largely different between each side of the fault; in the northwestern side, deciduous broad-leaved forest was predominant, while in the other side, coniferous forest was extensively distributed. In areas around Gengda Fault, deciduous forest

prevailed in the northwestern side of the fault; however, farmland also occupied a large area. Vegetation in the other side of Gengda Fault was more various because broad-leaved forest, coniferous forest, shrub, and meadow were mixed, without an obvious dominant type.

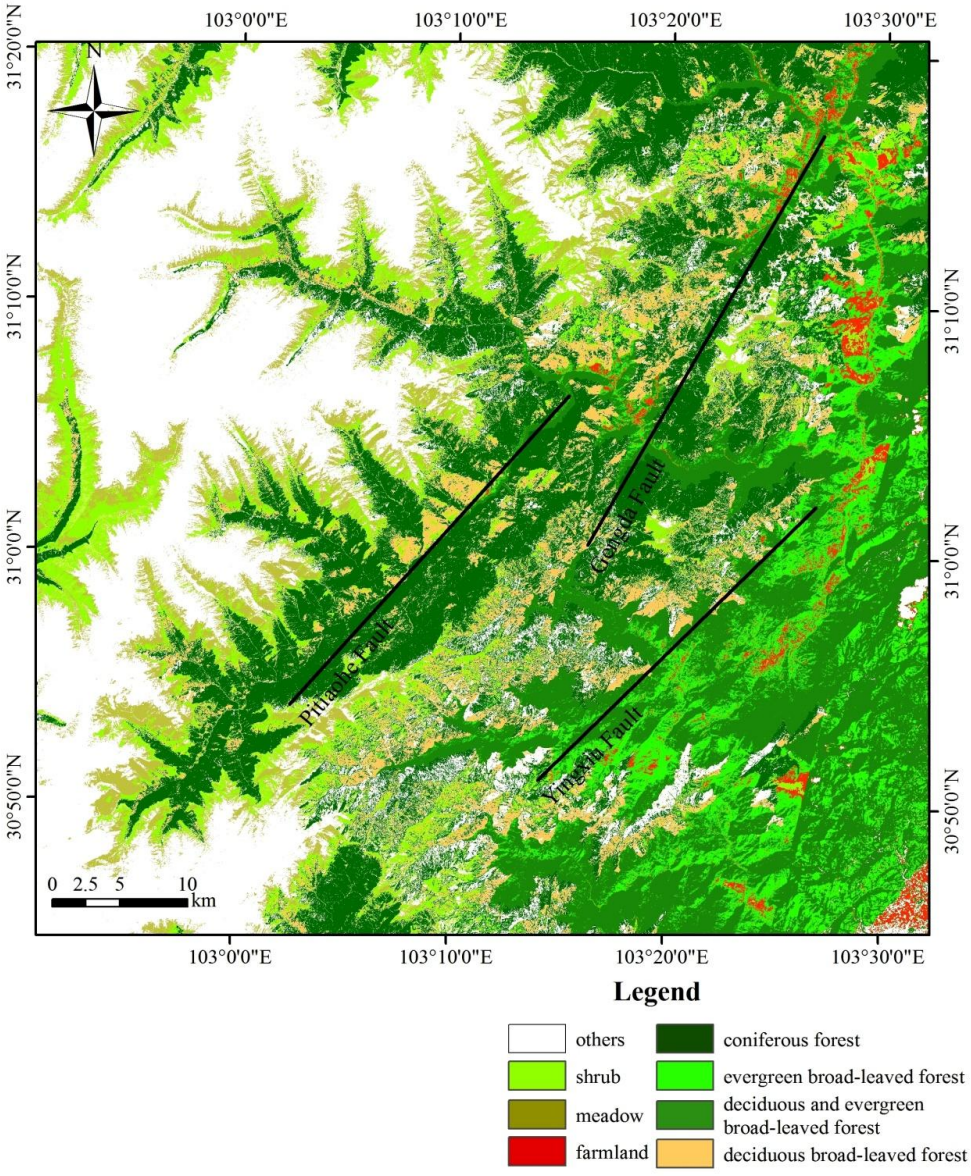


Fig. 4.3. Distribution of seven vegetation classes from an advanced land observing satellite image acquired on 1 February 2007 classified by a hybrid unsupervised-supervised approach.

To further examine the positional relationship between the vegetation pattern and the fracture zones, distribution areas of each vegetation type were combined with the graded lineament density (Fig. 4.3). Lineament gradation was defined based on the quartile of cumulative distribution of the lineament density. Change patterns associated with the lineament density could be found in broad-leaved forest and farmland. Their distributions increase with increasing lineament density until density level 6; after which, they decrease. The coverage of mixed forest and deciduous broad-leaved forest had a maximum at lineament density level 4. More noteworthy was that deciduous and evergreen broad-leaved forest became dominant in the areas where the lineaments were densely distributed, with density levels larger than 4. However, deciduous broad-leaved forest was often found in areas with low lineament density levels, such as those less than 4. The coverage of coniferous forest and shrub areas both gradually decreased with increasing lineament density. However, the relationship between meadow and lineament density was not clear because the change of the meadow distribution was small and not related to changes in lineament density. To summarize the results apparent from Fig. 4.3, broad-leaved forest, mixed forest and farmland persisted in areas with moderate levels of lineament density (levels 4–6). Deciduous broad-leaved forest and coniferous forest persisted in areas that are not strongly fractured (below level 4). Shrub and meadow were uniformly distributed over the whole range of lineament density levels.

However, in the most strongly fractured areas (level 8), shrub occupied the largest area and the distribution areas increased from farmland, broad-leaved forest, deciduous broad-leaved forest, mixed forest, meadow to coniferous forest (Fig. 4.5). Consequently,

forests were considered to be mainly distributed in less fractured areas, while farmland, shrub and meadow was found in areas with high fracture density.

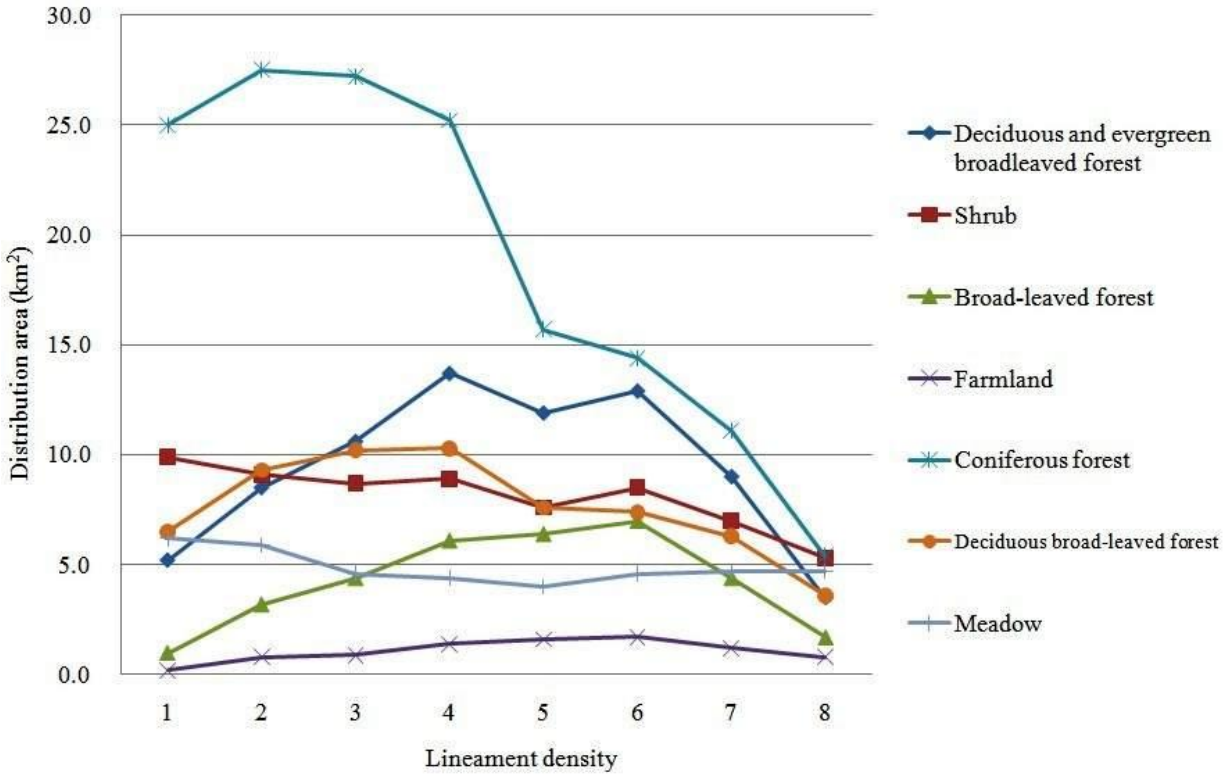


Fig. 4.4. Distribution areas of each vegetation type at each lineament density level

Table 4.1 Parameters of Variogram models on NDVI experimental semivariogram

| Area | Date | Model | Sill | Nugget effect | Minor range(m) | Major range(m) | Direction of major range |
|---|---|---|---|---|---|---|---|
| Whole | 5 April 2008 | Spherical | 0.015 | 0.016 | 21,000 | 35,000 | N33°E |
| I | 5 April 2008 | Exponential | 0.010 | Non | 805 | 1750 | N44°E |
| II | 5 April 2008 | Exponential | 0.011 | Non | 1500 | 2000 | N47°E |

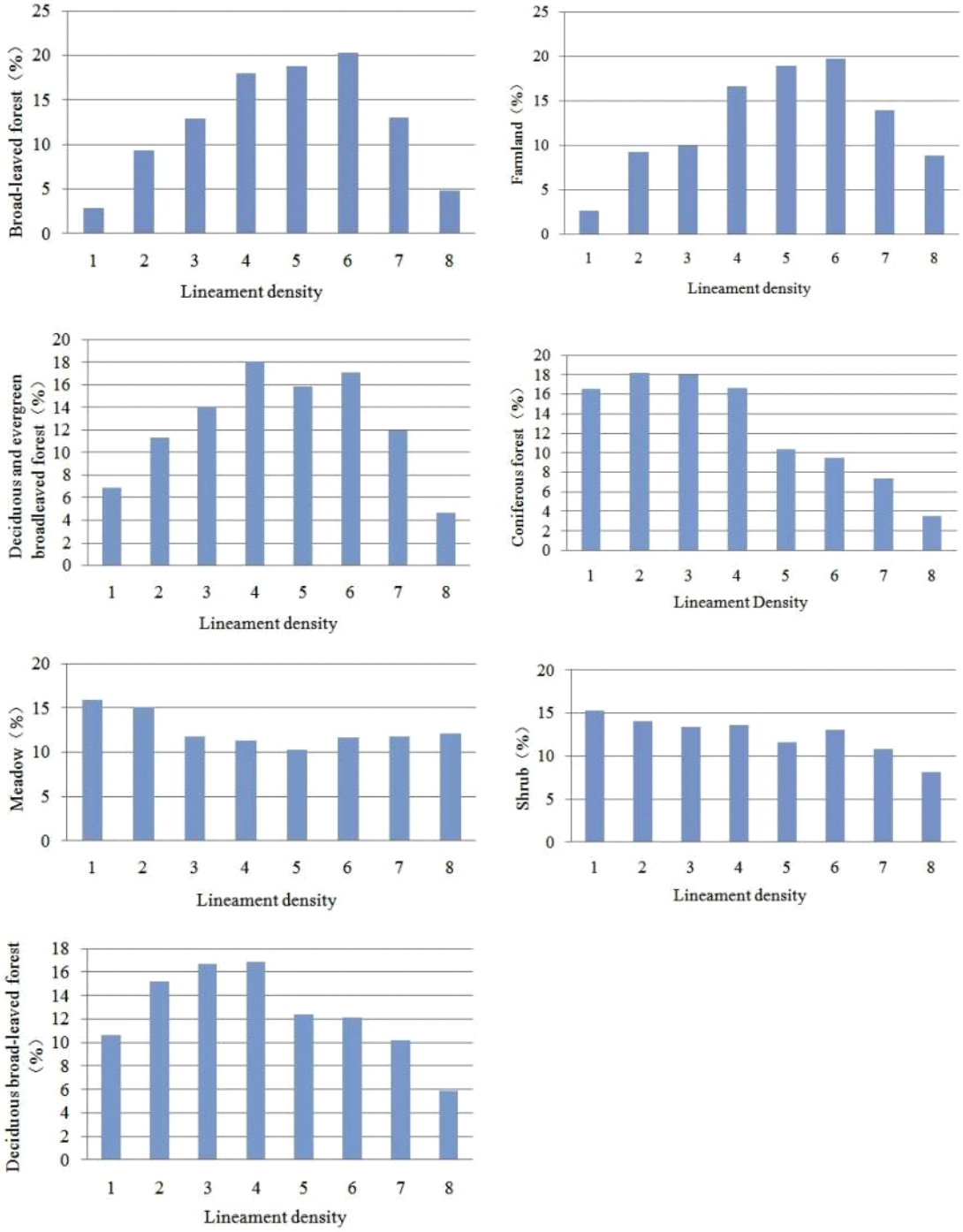


Fig. 4.5. Relationship between appearance percentage of each vegetation type and graded lineament density. Levels were defined from 1 to 8 in which 1 is the lowest density of lineaments and 8 is the highest density of lineaments.

## 4.4 Anisotropy of semivariogram

For semivariogram analysis, the average NDVI values of all pairs that have a similar distance and angle were plotted on a semivariogram surface as shown in Figs. 4.6 An ellipse overlain on each semivariogram surface represents the range at each direction; flatness of the ellipse becomes larger with increasing anisotropic strength of the semivariogram. Figures 4.6A and B show γ(h)s along the major and minor axes. Clearly, NDVI γ(h)s for all the study area before and after the earthquake can be adequately approximated by a spherical model (Figs. 4.6 A and B). Table 4.1 summarizes the parameters of the semivariogram models. The directions along the major ranges before the earthquake were N33°E, which noteworthy corresponds with the strikes of the fracture zones (N30-50°E).

Since the domain of the study area was extensive (66×66 km), factors that influence the vegetation patterns must be complicated. The above γ(h)s may not be suitable to express local heterogeneity of the vegetation pattern. According to Garrigues (2006), a 7×7 km extent can be appropriate for capturing ecological process. Thus, to examine whether the fracture zones affect the vegetation pattern, we selected two typical case study areas with both dimensions of 7×7 km, termed Areas I and II (see Fig. 2.2), which both included one river and one fault. Yuzixi River flowed through Area I from west to east and there was a detected fracture zone composed of Gengda Fault, passing through Area I with strike of about N30°E. Area II was characterized by being located at the end of Pitio River, which coincided with Pitiaohe Fault. Within Area I, the flow of Yuzixi River was almost perpendicular to the strike of Gengda Fault, while in area II, Pitiao River is parallel to Pitiaohe Fault.

(A) (B) (C)

Whole area: before the earthquake

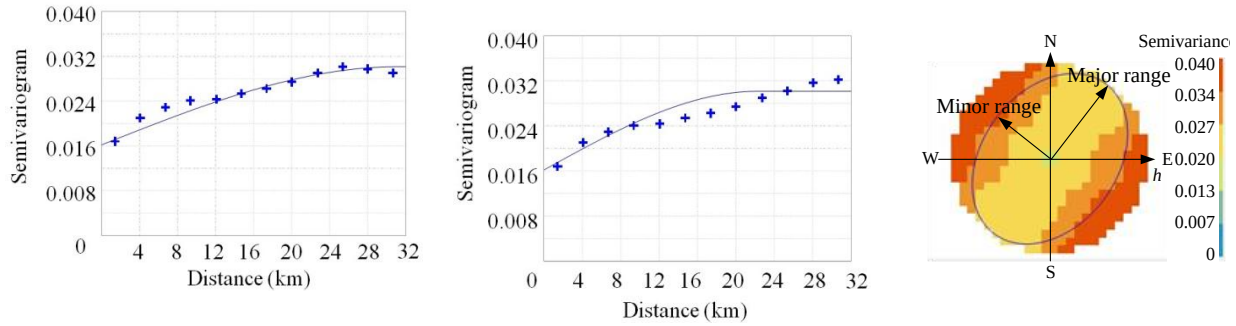


Area I: before earthquake

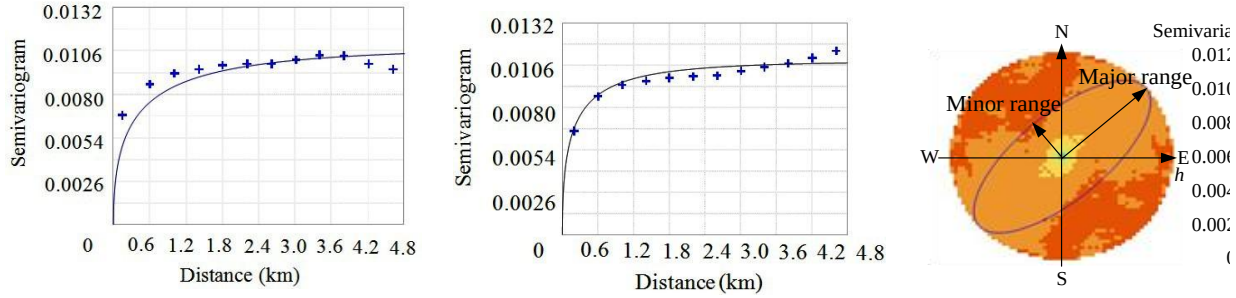


Area II: before earthquake

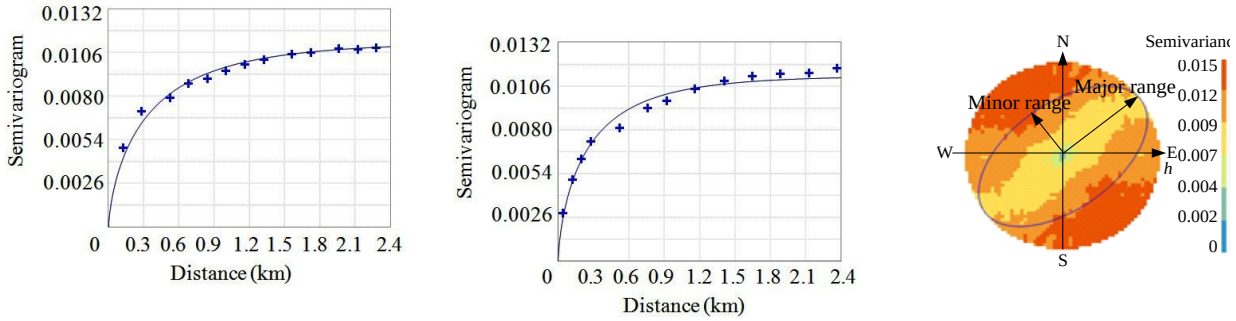


Fig. 4.6. Experimental semivariograms of NDVI data in the whole area, Areas I and II on dates before the Wenchuan earthquake. (A) semivariograms along the

major range and (B) along the minor range, and (C) semivariogram surfaces. Curves on the semivariograms express exponential models that approximate the trends. Ellipses on the semivariogram surfaces indicate the range at each direction.

Semivariogram surfaces (Fig. 4.6) clearly represent anisotropic behaviors of Areas I and II. All NDVI γ(h)s of the two case study areas were linear at the origin without nugget effects, which suggests that spatial variations within a pixel are small relative to environmental variations. They all converged to sills. Contrary to the γ(h) of whole area, the exponential model was the best fit to the γ(h)s of Areas I and II.

In terms of anisotropy, before the earthquake, the γ(h) of Area I increased largely near the origin and reached the sill at the major range of 1750 m along the direction of N44°E. On the other hand, the γ(h) of Area II reached the sill at major range of 2000 m along the direction of N47°E. Therefore, the vegetation patterns tended to be most continuous along these northeast directions in both the areas. This trend is harmonious with that of the anisotropic behavior of the whole study area. Taking the fracture zones into account, the trends of the vegetation patterns in the two areas both coincide with the strikes of the two fracture zones because the strikes of Gengda and Pitiaohe Faults were identified as N30-50°E by STA. As previously explained, Yuzixi River flowed through Area I from west to east, with a direction about N30°W, which was almost orthogonal with the strike of Gengda Fault. However, the result of the semivariogram clarified the coincident relationship between the vegetation pattern and the fracture zone. Consequently, in this area the fracture zones preponderate in influencing the vegetation patterns over the river in

this area the fracture zones influenced the vegetation patterns in the watersheds.

## 4.5 Conclusion

This chapter focuses on the relationship between fracture zones and distribution of vegetation cover types. A set of remote sensing and GIS techniques were adopted to make the classification map of vegetation, combine lineament with vegetation cover, and realize geostatistical analysis.

Firstly, NDVI on two dates were employed to represent vegetation and to be analyzed with lineament. Results show that values around either side of main fault are quite different, but appeared to be same trend along the fault, which initially indicate that vegetation cover type around the fracture zones might be different.

Analysis of vegetation type and lineament density showed that broad-leaved forest, mixed forest and farmland persisted in the areas with a moderate level of lineament density and deciduous broad-leaved forest and coniferous forest persisted in the less fractured areas. The relationship between the distributions of shrub and meadow and the lineament density was unclear. Meadow, farmland, shrub persisted in the strongly fractured areas.

To examine whether the fracture zones affected the vegetation pattern, two typical areas, which both included one river and one fault, with dimensions of 7×7 km, were selected. The trend of vegetation pattern identified from the anisotropy of NDVI semivariograms shows that the most continuous directions were northeast in both areas, which was consistent with those of the strikes of fracture zones in the two areas.

## References

Brown, D., Danial, G., 1994. Predicting vegetation types at treeline using topography and biophysical disturbance. Journal of Vegetation Science, 5:641-656.

China Geological Survey, 1996. Spatial database of 1:500,000 digital geological map of The People's Republic of China.

Chigira, M., Wu, X., Inokuchi, T., Wang, G., 2010. Landslides induced by the 2008 Wenchuan earthquake, Sichuan, China. Geomorphology, 118: 225-238.

Davis, G., 1984. Structural Geology of Rocks and Regions, Wiley, New York, 475.

Garrigues, S., Allard, D., Baret, F., 2006. Quantifying spatial heterogeneity at the landscape scale using variogram model. Remote Sensing of Environment, 103: 81-96.

Gao, Z., Liu, J., 2000. The study on driving factors and models of NDVI change based on remote sensing and GIS in China. Climatic and Environmental Research, 5(2):155-164.

Hara, M., Hirata, K., Fujihara, M., and Oono, K., 1996. Vegetation structure in relation to micro-landform in an evergreen broad-leaved forest on Amami Ohshima Island, Southwest Japan. Ecological Research, 11:325-337.

Henebry, G., 1993. Detecting change in grasslands using measures of spatial dependence with Landsat TM. Remote Sensing of Environment, 46: 233-234.

Huang, R., Li, W., 2008. Development and distribution of geohazards triggered by 5.12 Wenchuan earthquake in China. Science in China Series E: Technical Science, 52:810-819.

Journel, A. G., Huijbregts, C., 1978. Mining Geostatistics, Academic Press, San Diego, 600.

Koike, K., Nagano, S., Ohmi, M., 1995. Lineament analysis of satellite images using a Segment Tracing Algorithm (STA). Computers and Geosciences, 21(9):1091-1104.

Koike, K., Nagano, S., Kawaba, K., 1998. Construction and analysis of interpreted fracture planes through combination of satellite-image derived lineaments and digital elevation model data. Computers and Geosciences, 24(6):573-583.

Lin, W., Lin, C., Chou, W., 2006. Assessment of vegetation recovery and soil erosion at landslides caused by a catastrophic earthquake: a case study in central Taiwan. Ecol. Eng., 28:79-89.

Masoud, A., Koike, K., 2006. Tectonic architecture through Landsat-7 ETM+/SRTM DEM-derived lineaments and relationship to hydrogeologic setting in Siwa region, NW Egypt. Journal of African Earth Sciences, 45:467-477.

Masoud, A., Koike, K., 2011. Auto-detection and integration of tectonically significant lineaments from SRTM DEM and remotely-sensed geophysical data. ISPRS Journal of Photogrammetry & Remote Sensing.

Matsushita, B., Yang, W., Chen, J., 2007. Sensitivity of the Enhanced Vegetation Index (EVI) and Normalized Difference Vegetation Index (NDVI) to topographic effect: A case study in high-density cypress forest. Sensors, 7:2636-2651.

O'Learly, D., Friedman, J., Pohn, H., 1976. Lineament, linear, lineation: some proposed new standards for old terms, Bulletin of the Geological Society of America, 87:1463-1469.

Ouimet, W., 2010. Landslides associated with the May 12, 2008 Wenchuan earthquake: Implications for the erosion and tectonic evolution of the Longmen Shan. Tectonophysics, 491:244–252.

Qu, Z., 1984. Plant Ecology. Higher Education Press, Beijing, 45-50.

Ruland, W., Cherry, J., Feenstra, S., 1991. The depth of fractures and active ground-water flow in a clayey till plain in southwestern ontario. Ground Water, 29(3): 405-417.

Sellers, P., 1985. Canopy reflectance, photosynthesis and transpiration. Int. J. Remote Sens., 6: 1335–1372.

Tang, H., Jia, H., Hu, X., Li, D., Xiong, C., 2010. Characteristics of landslides induced by the great Wenchuan earthquake. Journal of Earth Science, 21: 104-113.

Wang, L., Koike, K., Masoud, A., 2011. Relationship between remotely-sensed vegetation change and fracture zones induced by the 2008 Whenchuan Earthquake, China Journal of Earth Science (Springer: under second review).

Wang, L., Koike, K., 2010. Geostatistical approach to spatial heterogeneity change of vegetation cover around fracture zones. Proceeding of International Symposium on Earth Science and Technology, Fukuoka, December 7-8, pp. 479-484.

# Chapter 5

# Quantification of the Special Heterogeneity Change of Vegetation Pattern

## 5. 1 Introduction

The 2008 Wenchuan earthquake, with magnitude 8.0 Ms according to the China Earthquake Administration, caused huge damages to infrastructure and human fatalities. Moreover, many of natural resources were ruined during the earthquake. In addition to the direct destruction and devastation wrought by the earthquake itself, the ensuing second disasters such as landslides and debris flows are responsible for the horrifying aftermath scenes (Huang et al., 2008; Chigira et al., 2010; Tang et al., 2010; Fan et al., 2010). All these disturbances consequently destructed the ecosystem.

Special heterogeneity is one structural feature of ecological systems. It can be defined as the complexity and variability of a system property in time and space. A system property in this case can be nearly any measurable entity, such as the configuration of the landscape mosaic, plant biomass, annual precipitation, or soil nutrient concentrations (Li, 1994; Turner, et al., 1991). Li (1994) proposed operational definitions for spatial heterogeneity in both categorical and numerical landscape maps. Spatial heterogeneity in categorical landscape maps is defined as the complexity in both composition (which is non spatial) and configuration (which is spatial) of patch. Composition implies which categories are present and how much of the categories there are, ignoring the specific spatial arrangement of the categories on the landscape. Configuration refers to the specific spatial arrangement of different cover types on a landscape.

As for variability of spatial heterogeneity, Burrough (1986) proposed that spatial heterogeneity in numerical landscape maps is continuum of degrees of variability in domain variation, autocorrelated variation, and random noise. Garrigues et al. (2006)

provided detailed definitions of variability of spatial heterogeneity measured from remote sensing sensors, which is described through two components: (1) spatial variability of the surface property over the observed scene and (2) spatial structures. They are defined as patches or objects that repeat themselves independently within the observed scene at a characteristic length scale which represents the extent of the spatial structure. They can be viewed as the typical correlation area of the surface property. Spatial structures within remotely sensed images are identifiable in that their spectral properties are more homogeneous within them than between them and other scene elements data are often distributed into independent sets of spatial structures, related to different length scales and spatial variability, being overlaid in the same region.

To monitor ecosystem changes after and before the earthquake at landscape scale, we need to quantify the system structure of interest to determine the magnitude and rate of change (O'Neill et al., 1988; Turner and Gardner, 1991). Quantification of spatial heterogeneity is a promising way of examining structure of ecological systems (O'Neill et al.,1991). The fundamental premise is that spatial heterogeneity may have great effects on functions and processes of ecological systems and these changes in spatial heterogeneity may reflect changes in functions and processes (Risser et al., 1984; Forman and Godron, 1986; Kolasa and Pickett, 1991; Turner and Gardner, 1991).

Accordingly, in this chapter, we intend to quantify the spatial heterogeneity and analyze its changes disturbed by the earthquake in terms of both categorical map and numerical maps. Such analysis is bound to provide comprehensive understanding of spatial heterogeneity change in the study area, which is expected to provide the theoretical base

for the future sustainable forest resource management and local development. Moreover, this study may be also useful for researchers who are studying the habitats of giant panda.

## 5.2 Method

In order to examine complexity of spatial heterogeneity in categorical landscape maps, several landscape metrics were employed both for composition and configuration analysis. Fragstats 3.3 was utilized to be the software calculating the landscape metrics selected in this study. Patches form the basis for categorical maps. Commonly, landscape metrics may be defined at three levels: Patch-level metrics, Class-level metrics and Landscape-level metrics. Patch-level metrics are defined for individual patches, and characterize the spatial character and context of patches. In most applications, patch metrics serve primarily as the computational basis for several of the landscape metrics.

Class-level metrics are integrated over all the patches of a given type (class). There are additional aggregate properties at the class level that result from the unique configuration of patches across the landscape. In many applications, the primary interest is in the amount and distribution of a particular patch type. A good example is in the study of habitat fragmentation. Habitat fragmentation is a landscape-level process in which contiguous habitat is progressively sub-divided into smaller, geometrically more complex (initially, but not necessarily ultimately), and more isolated habitat fragments as a result of both natural processes and human land use activities (McGarigal and McComb 1995). This process involves changes in landscape composition, structure, and function and occurs on a backdrop of a natural patch mosaic created by changing landforms and natural disturbances. Habitat loss and fragmentation is the prevalent trajectory of landscape change in several

human-dominated regions of the world, and is increasingly becoming recognized as a major cause of declining biodiversity (Burgess and Sharpe 1981, Whitcomb et al. 1981, Noss 1983, Harris 1984, Wilcox and Murphy 1985, Terborgh 1989, Noss and Cooperrider 1994). Class indices separately quantify the amount and spatial configuration of each patch type and thus provide a means to quantify the extent and fragmentation of each patch type in the landscape.

Landscape-level metrics are integrated over all patch types or classes over the full extent of the data. In many applications, the primary interest is in the pattern (i.e., composition and configuration) of the entire landscape mosaic. A good example is in the study of wildlife communities. Aldo Leopold (1933) noted that wildlife diversity was greater in more diverse and spatially heterogeneous landscapes. Thus, the quantification of landscape diversity and heterogeneity has assumed a preeminent role in landscape ecology. Indeed, the major focus of landscape ecology is on quantifying the relationships between landscape pattern and ecological processes. Consequently, much emphasis has been placed on developing methods to quantify landscape pattern (e.g., O'Neill et al. 1988, Li 1990, Turner 1990, Turner and Gardner 1991) and a great variety of landscape-level metrics have been developed for this purpose.

There are extensive set of landscape metrics, in this study, we evaluated the following indices in both class-level and landscape-level: Total (Class) area (CA/TA), Number of Patches (NP), Patch Density (PD), Largest Patch Index (LPI), Landscape Shape Index (LSI), Patch Richness (PR), Clumpiness Index (CLUMPY), Shannon's Diversity Index (SHDI), Fracture Dimension (FD), Shannon's evenness Index (SHEI) and Contagion (CONTAG).These metrics were chosen because they are commonly used in landscape

ecology and seem to represent different spatial heterogeneity components. The equations and ecological significance of each index are modified from fragstats (McGarigal and McComb, 2002). The equations and ecological significance of each index is listed as follows:

1. Class Area

$$CA = \sum_{j=1}^{a} a_{ij} \left(\frac{1}{10{,}000}\right) \quad (1)$$

where $a_{ij}$ = area ($m^2$) of patch ij.

CA equals the sum of the areas ($m^2$) of all patches of the corresponding patch type, divided by 10,000 (to convert to hectares); that is, total class area. The unit of CA is hectares. The value of CA is more than 0, without limit.

Ecological significance: Class area is a measure of landscape composition; specifically, how much of the landscape is comprised of a particular patch type. In addition to its direct interpretive value, class area is used in the computations for many of the class and landscape metrics.

2. Number of Patches

$$NP = n_i \quad (2)$$

Where $n_i$ = number of patches in the landscape of patch type (class) i.

NP equals the number of patches of the corresponding patch type (class). NP is Greater than or equal to 1, without limit.

Ecological significance: Number of patches of a particular patch type is a simple measure of the extent of subdivision or fragmentation of the patch type. Although the number of patches in a class may be fundamentally important to a number of ecological processes, often it has limited interpretive value by itself because it conveys no information about area, distribution, or density of patches. Of course, if total landscape area and class area are held constant, then number of patches conveys the same information as patch density or mean patch size and may be a useful index to interpret. Number of patches is probably most valuable, however, as the basis for computing other, more interpretable, metrics. Note that the choice of the 4-neighbor or 8-neighbor rule for delineating patches will have an impact on this metric.

3. Patch density

$$PD = \frac{n_i}{A}(10{,}000)(100) \qquad (3)$$

Where $n_i$ = number of patches in the landscape of patch type (class) i.

A = total landscape area ($m^2$).

PD equals the number of patches of the corresponding patch type divided by total landscape area (m2), multiplied by 10,000 and 100 (to convert to 100 hectares). The unit is number per 100 hectares. The value of patch density is always more than 0.

Patch density is a limited, but fundamental, aspect of landscape pattern. Patch density has the same basic utility as number of patches as an index, except that it expresses

number of patches on a per unit area basis that facilitates comparisons among landscapes of varying size. Of course, if total landscape area is held constant, then patch density and number of patches convey the same information. Like number of patches, patch density often has limited interpretive value by itself because it conveys no information about the sizes and spatial distribution of patches.

4. Landscape Shape Index

$$LSI = \frac{e^i}{min e^i} \quad (4)$$

Where $e_i$ = total length of edge (or perimeter) of class i in terms of number of cell surfaces; includes all landscape boundary and background edge segments involving class i.

min $e_i$ = minimum total length of edge (or perimeter) of class i in terms of number of cell surfaces (see below).

LSI equals the total length of edge (or perimeter) involving the corresponding class, given in number of cell surfaces, divided by the minimum length of class edge (or perimeter) possible for a maximally aggregated class, also given in number of cell surfaces, which is achieved when the class is maximally clumped into a single, compact patch.

LSI = 1 when the landscape consists of a single square or maximally compact (i.e., almost square) patch of the corresponding type; LSI increases without limit as the patch type becomes more disaggregated (i.e., the length of edge within the landscape of the corresponding patch type increases).

Ecological significance: Landscape shape index provides a simple measure of class aggregation or clumpiness

5. Largest Patch Index

$$LPI = \frac{\max_{j=1}^{a}(a_{ij})}{A}(100) \quad (5)$$

where $a_{ij}$ = area ($m^2$) of patch ij.

A = total landscape area ($m^2$).

LPI equals the area ($m^2$) of the largest patch of the corresponding patch type divided by total landscape area ($m^2$), multiplied by 100 (to convert to a percentage); in other words, LPI equals the percentage of the landscape comprised by the largest patch. The unit of LPI is percent. The value of LPI is between 0 and 100.

LPI approaches 0 when the largest patch of the corresponding patch type is increasingly small. LPI = 100 when the entire landscape consists of a single patch of the corresponding patch type; that is, when the largest patch comprises 100% of the landscape.

Ecological significance: Largest patch index at the class level quantifies the percentage of total landscape area comprised by the largest patch. As such, it is a simple measure of dominance.

6. Patch Richness

$$PR = m \quad (6)$$

Where m = number of patch types (classes) present in the landscape, excluding the landscape border if present.

PR equals the number of different patch types present within the landscape boundary. The value of PR is greater or equal to 1, without limit.

Ecological significance: Patch richness is perhaps the simplest measure of landscape composition, but it does not reflect the relative abundances of patch types.

7. Shannon's Diversity Index

$$SHDI = -\sum_{i=1}^{m} P_i * \ln P_i \qquad (7)$$

where $P_i$ = proportion of the landscape occupied by patch type (class) i.

SHDI equals minus the sum, across all patch types, of the proportional abundance of each patch type multiplied by that proportion. The value of SHDI is greater or equal to 0, without limit.

Ecological significance: SHDI = 0 when the landscape contains only 1 patch (i.e., no diversity). SHDI increases as the number of different patch types (i.e., patch richness, PR) increases and/or the proportional distribution of area among patch types becomes more equitable.

Shannon’s diversity index is a popular measure of diversity in community ecology, applied here to landscapes.

8. Shannon's Evenness Index

$$SHEI = \frac{-\sum_{i=1}^{m} P_i * ln\, P_i}{\ln m} \qquad (8)$$

where $P_i$ = proportion of the landscape occupied by patch type (class) i.

m= number of patch types (classes) present in the landscape, excluding the landscape border if present.

SHEI equals minus the sum, across all patch types, of the proportional abundance of each patch type multiplied by that proportion, divided by the logarithm of the number of patch types. In other words, the observed Shannon's Diversity Index divided by the maximum Shannon's Diversity Index for that number of patch types. The value of SHEI is between 0 and 1.

Ecological significance: SHDI = 0 when the landscape contains only 1 patch (i.e., no diversity) and approaches 0 as the distribution of area among the different patch types becomes increasingly uneven (i.e., dominated by 1 type). SHDI = 1 when distribution of area among patch types is perfectly even (i.e., proportional abundances are the same).

Shannon's evenness index is expressed such that an even distribution of area among patch types results in maximum evenness. As such, evenness is the complement of dominance.

9. Contagion

$$CONTAG = \left[1 + \frac{\sum_{i=1}^{m}\sum_{k=1}^{m}\left[(P_i)\left(\frac{g_{ik}}{\sum_{k=1}^{m} g_{ik}}\right)\right] * \left[ln(P_i)\left(\frac{g_{ik}}{\sum_{k=1}^{m} g_{ik}}\right)\right]}{2\ln(m)}\right](100) \qquad (9)$$

Where $P_i$ = proportion of the landscape occupied by patch type (class) i.

$g_{ik}$ = number of adjacencies (joins) between pixels of patch types (classes) i and k based on the double-count method.

m = number of patch types (classes) present in the landscape, including the landscape border if present.

CONTAG equals minus the sum of the proportional abundance of each patch type multiplied by the proportion of adjacencies between cells of that patch type and another patch type, multiplied by the logarithm of the same quantity, summed over each unique adjacency type and each patch type; divided by 2 times the logarithm of the number of patch types; multiplied by 100 (to convert to a percentage). In other words, the observed contagion over the maximum possible contagion for the given number of patch types. The unit of CONTAG is percent. The value is between 0 and 100

CONTAG approaches 0 when the patch types are maximally disaggregated (i.e., every cell is a different patch type) and interspersed (equal proportions of all pairwise adjacencies). CONTAG = 100 when all patch types are maximally aggregated; i.e., when the landscape consists of single patch.

Contagion is inversely related to edge density. When edge density is very low, for example, when a single class occupies a very large percentage of the landscape, contagion is high, and vice versa. In addition, note that contagion is affected by both the dispersion and interspersion of patch types. Low levels of patch type dispersion (i.e., high proportion of like adjacencies) and low levels of patch type interspersion (i.e., inequitable distribution of pairwise adjacencies results in high contagion, and vice versa.

10. Perimeter-area fractal dimension

$$PAFRAC = \frac{2}{\frac{\left[N\sum_{i=1}^{m}\sum_{j=1}^{n} ln\,P_{ij} * ln\,a_{ij}\right] - \left[\left(\sum_{i=1}^{m}\sum_{j=1}^{n} ln\,P_{ij}\right) * \left(\sum_{i=1}^{m}\sum_{j=1}^{n} ln\,a_{ij}\right)\right]}{\left(N\sum_{i=1}^{m}\sum_{j=1}^{n} ln\,P_{ij}^{2}\right) - \left(\sum_{i=1}^{m}\sum_{j=1}^{n} ln\,P_{ij}\right)^{2}}} \quad (10)$$

$a_{ij}$ = area ($m^2$) of patch ij.

$p_{ij}$ = perimeter (m) of patch ij.

N = total number of patches in the landscape.

PAFRAC equals 2 divided by the slope of regression line obtained by regressing the logarithm of patch area ($m^2$) against the logarithm of patch perimeter (m). The value of PAFRAC is between 1 and 2.

A fractal dimension greater than 1 for a 2-dimensional landscape mosaic indicates a departure from a Euclidean geometry (i.e., an increase in patch shape complexity). PAFRAC approaches 1 for shapes with very simple perimeters such as squares, and approaches 2 for shapes with highly convoluted, plane-filling perimeters. PAFRAC employs regression techniques and is subject to small sample problems. Specifically, PAFRAC may exceed the theoretical range in values when the number of patches is small (e.g., <10), and its use should be avoided in such cases. In addition, PAFRAC requires patches to vary in size.

Perimeter-area fractal dimension at the landscape level is identical to the class level (see previous comments), except here all patches in the landscape are included in the regression of patch area against patch perimeter.

## 5.3. Results

### 5.3.1 Spatial heterogeneity characteristics

**(1) Categorical map**

The structure of the alpine environment is often characterized by assessing the pattern and composition of plant productivity and cover type information (Brown, 1994; Walsh et al., 1994). Landscape types in the this study area comprises coniferous forest, broad-leaved forest, deciduous forest, mixed forest, farmland, others (ice, snow and bare land) before the earthquake (Fig.5.1.a); as for one that after the earthquake, an additional

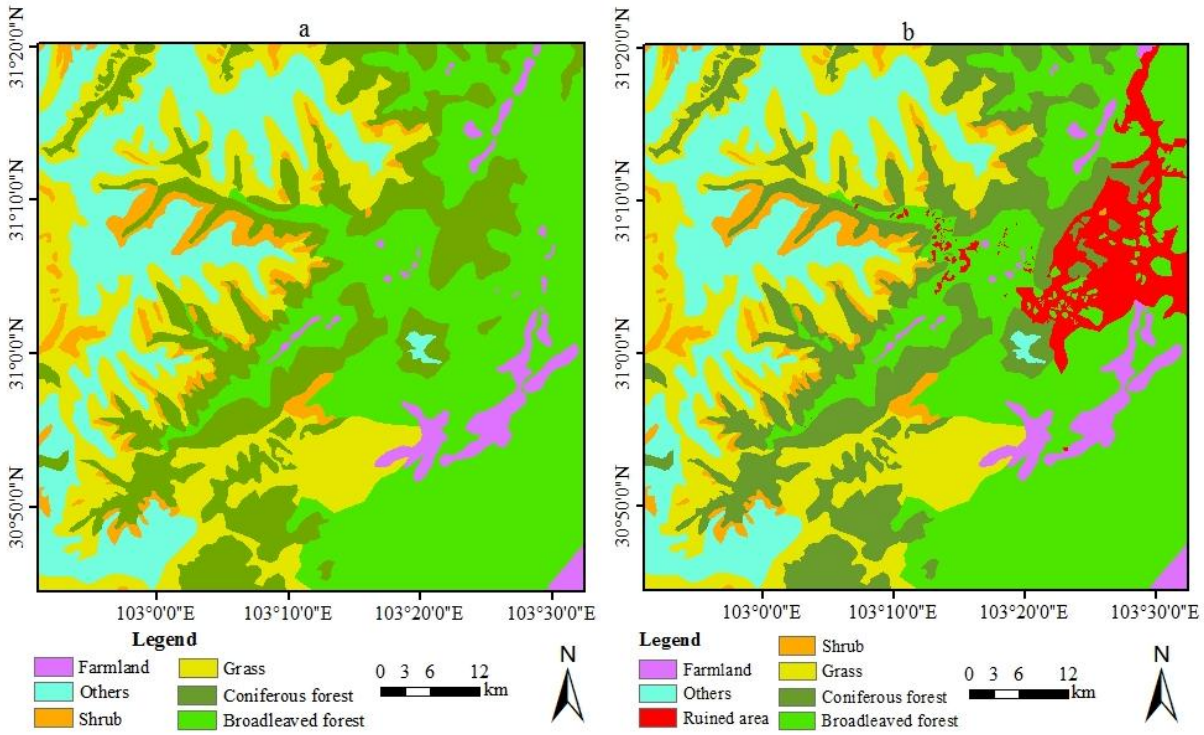


Fig. 5.1. Vegetation type maps interpreted from two images of Landsat ETM+ data before (5 April 2008) and after (23 May 2008) the Wenchuan earthquake. (a) vegetation type map before the earthquake and (b) after the earthquake.

landscape type, namely ruined area, was involved to discriminate areas that destructed by the earthquake from normal non-vegetated areas (Fig.5.1.b).

Six landscape metrics were utilized to quantify the spatial heterogeneity before and after the earthquake both at class-level and landscape-level. Spatial heterogeneity of each landscape type is well characterized and depicted by Table 5.1, Table 5.2 and Figure 5.4. Area of broad-leaved forest is 149590.4 hectare, ranking the first among all landscape types. Following ones are grass and coniferous forest respectively (Table.5.1). Landscape types after the earthquake have the same order in area amount with the ones before the earthquake, although areas of coniferous forest and broad-leaved forest decrease surviving from the earthquake. Besides, shrub and grass increase in area through the earthquake. Area of farmland decrease a little after the earthquake (Fig.5.2). Most of the landscape component types increase in patch number, especially broad-leaved forest, which increases from 2 to 42 after the earthquake (Table5.1 & Table 5.2). Change of patch density shows the same pattern among the landscape types with patch number. As for largest patch index, all the class appear to change little or remain the same except for broad-leaved forest, which decreases sharply from 34.22 to 22.87. Except farmland, all the other categories increase more or less in largest shape index. Clumpiness of all classes has tiny change comparing the value before and after the earthquake.

Table 5.3 summarizes the results of landscape metrics selected to quantify spatial heterogeneity of the study area at landscape-level. Each of the index representing different types of measure of spatial heterogeneity changes after the earthquake.

In order to understand how each landscape type change after the earthquake, a transfer matrix was made (Table 5.4). Area of 210 km2 of broad-leaved forest has been

Table 5.1. Characteristics of spatial heterogeneity of vegetation at Class-lever before the earthquake

| | Landscape metrics | | | | | |
|---|---|---|---|---|---|---|
| landscape type | CA | NP | PD | LPI | LSI | CLUMPY |
| coniferous forest | 89724.87 | 33 | 0.0076 | 5.8417 | 12.3791 | 0.972 |
| broad-leaved forest | 149590.4 | 2 | 0.0005 | 34.2206 | 6.2757 | 0.991 |
| Shrub | 18595.26 | 61 | 0.014 | 1.2891 | 13.1253 | 0.983 |
| Grass | 92625.57 | 8 | 0.0018 | 5.8972 | 14.3041 | 0.986 |
| Farmland | 13713.93 | 26 | 0.006 | 1.0478 | 7.265 | 0.994 |
| others | 71349.75 | 6 | 0.0014 | 11.8423 | 7.8928 | 0.983 |

Table 5.2. Spatial heterogeneity change of vegetation at landscape-lever before and after the earthquake

| | landscape type | | | | | | | | |
|---|---|---|---|---|---|---|---|---|---|
| Date | NP | PD | LPI | LSI | PAFRAC | CONTAG | PR | SHDI | SHEI |
| 20080405 | 136 | 0.03 | 34.22 | 12.04 | 1.37 | 58.21 | 6 | 1.56 | 0.87 |
| 20080523 | 226 | 0.05 | 22.86 | 13.71 | 1.27 | 54.16 | 7 | 1.71 | 1.17 |

ruined to be bare land. Correspondingly, 45 km2 of coniferous forest was ruined. Damaged area of farmland and grass is relatively slight.

Table 5.3. Characteristics of spatial heterogeneity of vegetation at Class-lever after the earthquake

| | landscape type | | | | | |
|---|---|---|---|---|---|---|
| landscape type | CA | NP | PD | LPI | LSI | CLUMPY |
| coniferous forest | 85148.55 | 33 | 0.0085 | 4.8101 | 12.9306 | 0.985 |
| broad-leaved forest | 129797.5 | 2 | 0.0096 | 22.8653 | 8.9413 | 0.991 |
| Shrub | 18661.14 | 61 | 0.0142 | 1.2891 | 13.1855 | 0.972 |
| Grass | 92660.04 | 8 | 0.0018 | 5.8972 | 14.3103 | 0.983 |
| Farmland | 13713.93 | 20 | 0.0046 | 1.0723 | 6.7641 | 0.984 |
| others | 71349.75 | 6 | 0.0014 | 11.8423 | 7.8928 | 0.991 |
| ruined area | 24917.58 | 51 | 0.0117 | 5.44 | 8.8623 | 0.984 |

Table 5.4. Transfer matrix of each vegetation type before and after the earthquake

| | 20080523 | | | | | | | |
|---|---|---|---|---|---|---|---|---|
| 20080405 | coniferous forest | broad-leaved forest | Shrub | Grass | Farmland | others | ruined area | Total |
| coniferous fores | 838.57 | 13.83 | 0.66 | 4.27 | - | - | 45.33 | 902.65 |
| broad-leaved forest | 12.85 | 1277.57 | - | 0.71 | 2.12 | - | 210.16 | 1503.40 |
| Shrub | - | - | 185.96 | 2.03 | - | - | - | 188.00 |
| Grass | - | 0.36 | 1.88 | 927.18 | - | - | 0.67 | 930.09 |
| Farmland | - | 4.91 | - | - | 128.56 | - | 4.14 | 137.61 |
| others | - | - | - | - | - | 713.42 | - | 713.42 |
| Total | 851.42 | 1296.67 | 188.50 | 934.19 | 130.68 | 713.42 | 260.30 | 4375.17 |

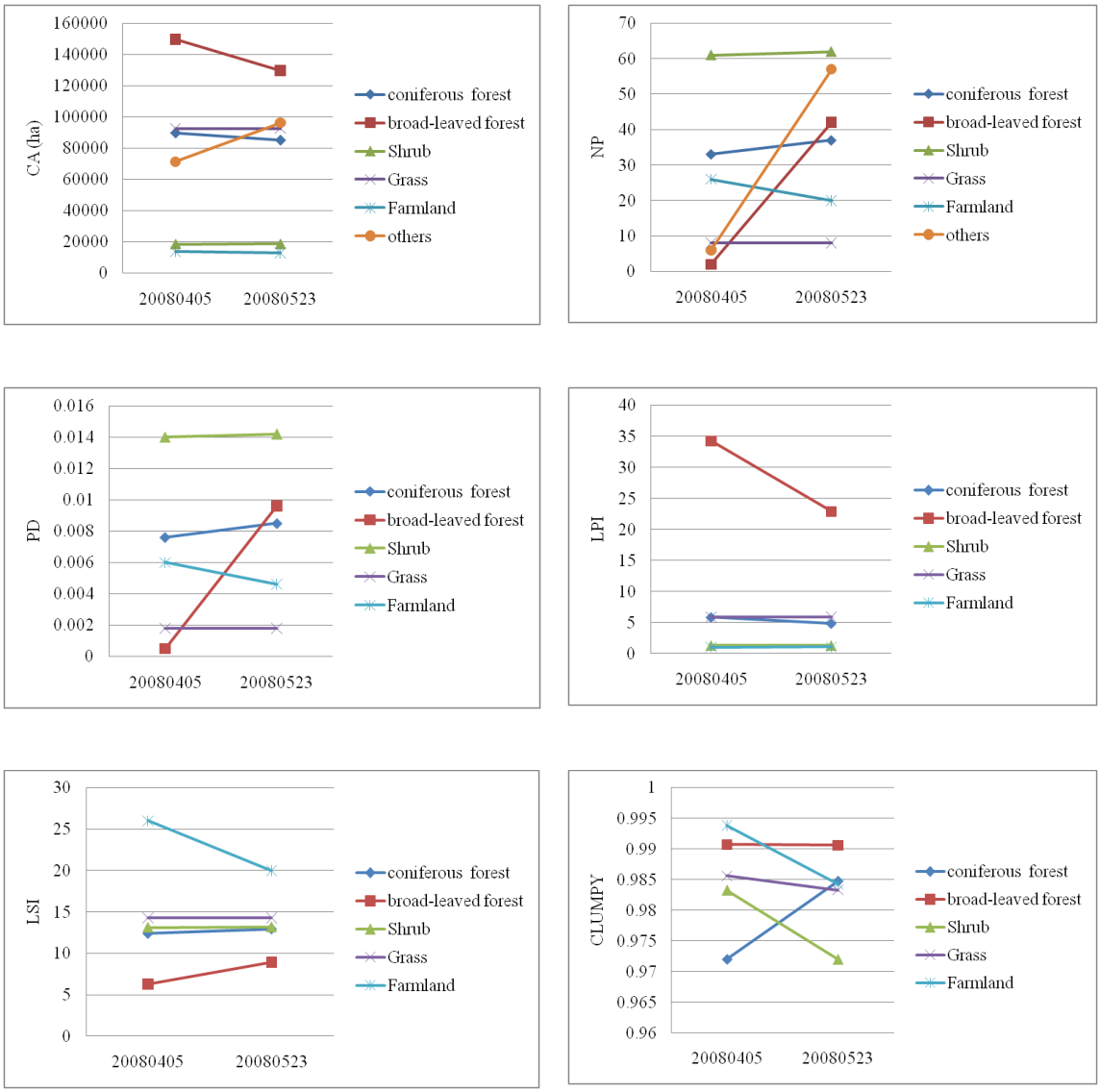


Fig. 5.2. Spatial heterogeneity change of each vegetation type at class lever quantified by landscape metrics at corresponding lever.

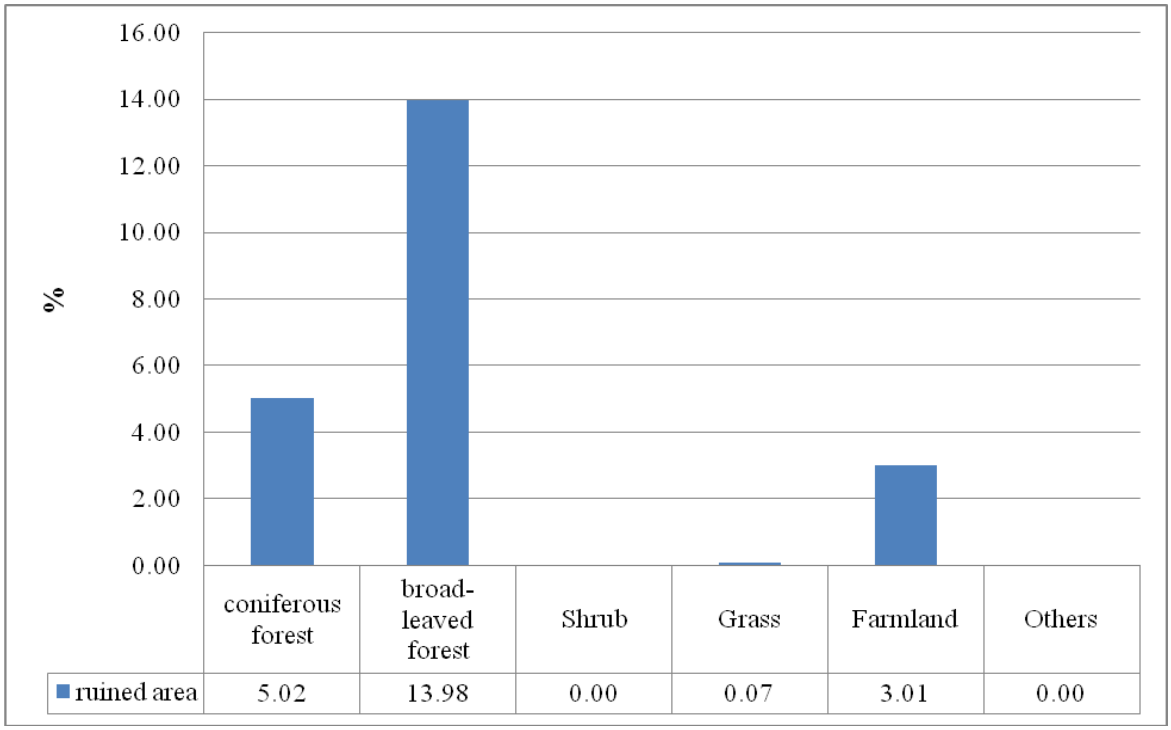


Fig. 5.3. Change percentage of each vegetation type to damaged area induced by the earthquake

**(2) Numerical map**

For semivariogram analysis, the average NDVI values of all pairs that have a similar distance and angle were plotted on a semivariogram surface as shown in Figs. 5.3. An ellipse overlain on each semivariogram surface represents the range at each direction; flatness of the ellipse becomes larger with increasing anisotropic strength of the semivariogram. Figures 4A and B show γ(h)s along the major and minor axes. Clearly, NDVI γ(h)s before and after the earthquake can be adequately approximated by a spherical model (Figs. 4A and B). All NDVI γ(h)s before and after the earthquake are linear at the origin They all converged to sills. Table 5.5 summarizes the parameters of the semivariogram models. The spatial variability is represented by the value of summation of

sill and nugget effect; it means that before the earthquake, the spatial variability is 0.031, while after the earthquake, the spatial variability increase to 0.067, more than twice than the one before the earthquake.

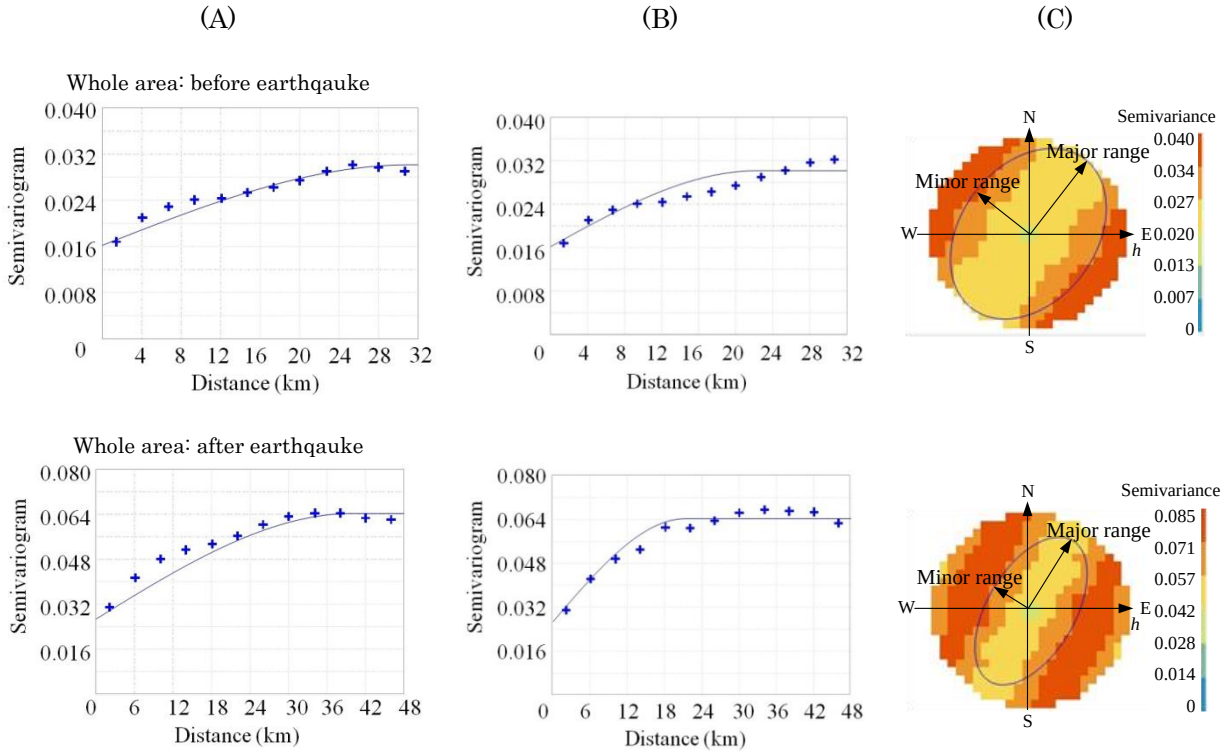


Fig. 5.4. Experimental semivariograms of NDVI data calculated from two images of Landsat ETM+ data before (5 April 2008) and after (23 May 2008) the Wenchuan earthquake over the study area. (A) semivariograms along the major range and (B) along the minor range, and (C) semivariogram surfaces when plotting the average values of data pairs separated by similar distances (shown by the length from the center) and angle at each azimuth (0–360°). Curves on the semivariograms express spherical models that approximate the trends. Ellipses on the semivariogram surfaces indicate the range at each direction.

The structure of spatial heterogeneity can be characterized by the range of semivariogram. According to the results summarized in table 5.4, both the minor range and major range of the NDVI-semivariogram increase after the earthquake, from 21 km to 25 km, and 35 km to 40 km respectively.

Table 5.5. Parameters of Variogram models on NDVZI experimental semivariogram

| Date | Model | Sill | Nugget effect | Minor range(m) | Major range(m) | Direction of major range |
|---|---|---|---|---|---|---|
| 5 April 2008 | Spherical | 0.015 | 0.016 | 21,000 | 35,000 | N33°E |
| 23 May 2008 | Spherical | 0.039 | 0.028 | 25,000 | 40,000 | N30°E |

In terms of anisotropy, before the earthquake, the $\gamma(h)$ increased largely near the origin and reached the sill at the major range along the direction of N33°E. The $\gamma(h)$ after the earthquake reached the sill at major range along the direction of N30°E, with slight change compared to one before the earthquake.

## 5.4 Discussion

### 5.4.1 Spatial heterogeneity change in terms of categorical map

**(1) Class-level change**

Class-lever metrics can quantify spatial heterogeneity of each vegetation type. Six types of landscape metrics were calculated on landscape maps before and after the earthquake to measure the change of each category. CA measure how much one particular

patch type is in the whole landscape. According to the result, forests are the main component types in this study area. It is conspicuous from the Figure 5.2 that areas of all kinds of forests decrease through the earthquake, though the changing magnitudes are more or less different. It is indicated from the result that broad-leaved forest was ruined most seriously among forests. Broad-leaved forest is widely distributed near the epicentre of the earthquake. Fig.5.3 shows change percentage of each landscape type to damaged area induced by the earthquake. Up to 14% of broad-leaved forests were ruined during the earthquake. Coniferous forest ranked second, with the ruined magnitude of 5%.

Number of patches of a particular patch type is a simple measure of the extent of subdivision or fragmentation of the patch type. Patch number of forest (i.e. coniferous forest and broad-leaved forest) increase the most among all landscape types after the earthquake (Table 5.1 & 5.2 and Fig. 5.2), suggesting serious fragmentation created by the earthquake. The same trend can be found in patch density. Broad-leaved forest took the maximum patch area but minimum patch number and density of patches before the earthquake, which indicate that broad-leaved forest is the main landscape type in this study area. Such extensive area of broad-leaved forest must play important role in the function of ecological system. However, due to the earthquake, area of broad-leaved forest has been dissected, which is indicated by patch number that largely changing from 2 to 42 (Table 5.1 and Table 5.2). Such change is bound to influence the ecosystem to some extent.

Largest patch index regards to the area of largest patch of the corresponding patch type. It is an indicator of dominance for all the landscape types. The values of broad-leaved forest are both the highest before and after the earthquake, suggesting its dominance in the area.  the magnitude of change for broad-leaved forest is also the greatest. Decreasing of

largest patch index also states that the areas were fragmented. The same trend can be also found in coniferous forest.

Landscape shape index equal to 1 when the landscape consists of a single square or maximally compact (i.e., almost square) patch of the corresponding type; LSI increases without limit as the patch type becomes more disaggregated. The value of landscape shape index increased for all the forest types by examining Table 1 and Table 5.2 and Fig. 5.2, which implied that all the forest types became more disaggregated influenced by Wenchuan earthquake.

**(2) Landscape-lever change**

Nine types of landscape-lever metrics were selected to measure the change of landscape before and after the earthquake in terms of both the composition and configuration.

Patch richness is the simplest measure of landscape composition. The total patch number increased from 136 to 226 through the earthquake. It indicates that the Wenchuan earthquake extremely aggravates the spatial heterogeneity in this area (Table 5.3). The value of Largest patch index also decrease largely. Landscape-level metrics correspond to all patch types over the whole area, with no sensitivity to single class. The increase of largest shape index indicates that the cover type tends to occur in isolated, dispersed grid cell or small patches.

Contagion measures aggregation of patch types. The relatively high value of contagion before the earthquake indicates that the patch types are aggregated better. Due to earthquake, contagion value decrease from 58 to 54. Shannon's diversity index measures

diversity of patch types. The value of SHDI increased from 1.56 to 1.71 after the earthquake. Fragmentation, a product of natural processes and anthropogenic activities, produces a landscape mosaic of interacting patches or polygons on a map coverage (Risser 1987; Turner 1989; Forman 1995). Consequently, landscape with more diverse habitat structure, combined with an unequal distribution and flow of resources, tend to contain greater species diversity (Tilman 1982; Forman and Godron 1986). However, in this case, the higher value of diversity only due to the patch richness which increased from 6 to 7. Shannon's evenness index increases. One reason for it is that the earthquake ruined some cover types which decreased their dominance in the area. Perimeter-area fractal dimension measures irregularity of patch shape in a landscape. The patch shape after the earthquake tends to be more regular, because the value of PAFRAC decreases according to the results.

### 5.4.2 Spatial heterogeneity change in terms of numerical map

The sill value of NDVI γ(h) can measure the magnitude of spatial variability of vegetation. The parameters listed in Table 5.5 show that the sill on 23 May 2008 was larger than that on 5 April 2008, which indicates that the spatial variability of vegetation pattern after the earthquake was greater than that before the earthquake. However, the minor range increased from 21km to 25km before and after the earthquake. The spatial correlations of NDVI on 23 May 2008 were stronger and longer than those of 5 April 2008 when comparing the shapes of γ(h)s (Fig. 5.4). This suggests that the earthquake uniformly decreased vegetation growth over a wide area. The sills of NDVI γ(h)s of the study area increased from 0.015 to 0.039 before and after the earthquake, which suggests that the Wenchuan earthquake caused the vegetation pattern to become more heterogeneous,

mainly by changing vegetation cover to bare land. Consequently, the semivariogram of NDVI proved to be a powerful tool to characterize and quantify the spatial variability of vegetation pattern.

## 5.5 Conclusion

The emphasis of chapter was placed on the quantification of the spatial heterogeneity and analysis of its changes disturbed by the earthquake. The research was conducted in tow aspects; categorical map and numerical maps.

Vegetation map before and after the earthquake were produced to be the basis data for quantifying spatial heterogeneity in term of categorical map. Ten landscape metrics were selected to quantify the SH in both class-level and landscape-level. The results from class-level indicated that forests get the most fragmentation due to the earthquake. Results from landscape-level revealed that the effect of earthquake on the spatial heterogeneity was obvious; the whole landscape tend to be more heterogeneity, the dominance decreased, and patch shape after the earthqauke inclined to be more irregular.

NDVI semivariograms were used to quantify the spatial heterogeneity in terms of the variability of change and spatial structure. It can be concluded from the result that the Wenchuan earthquake caused twice variability than before. Due to lots of vegetation changing to be bare land, range of the NDVI semivarigram increased after the earthquake.

## References

Brown, D., Danial, G., 1994. Predicting vegetation types at treeline using topography and biophysical disturbance. Journal of Vegetation Science, 5:641-656.

Burrough, P., 1986. Principles of geographical information systems for land resources assessment. Geocarto International. Vol. 1. Clarendon Press.

Chigira, M., Wu, X., Inokuchi, T., Wang, G., 2010. Landslides induced by the 2008 Wenchuan earthquake, Sichuan, China. Geomorphology, 118: 225-238.

China Geological Survey, 1996. Spatial database of 1:500,000 digital geological map of The People's Republic of China.

Fan, J., Chen, J., Tian, B., 2010. Rapid assessment of secondary disasters induced by the Wenchuan earthquake. Computing in Science & Engineering, 12(1):10-19.

Forman, R. T. T. 1995. Land Mosaics. Cambridge University Press. United Kingdom.

Forman, R. T. T. and Godron, M., 1986. Landscape Ecology. John Wiley & Sons, New York, 619.

Garrigues, S., Allard, D., Baret, F., 2006. Quantifying spatial heterogeneity at the landscape scale using variogram model. Remote Sensing of Environment, 103: 81-96.

Henebry, G., 1993. Detecting change in grasslands using measures of spatial dependence with Landsat TM. Remote Sensing of Environment, 46: 233-234.

Huang, R., Li, W., 2008. Development and distribution of geohazards triggered by 5.12 Wenchuan earthquake in China. Science in China Series E: Technical Science, 52:810-819.

Journel, A. G., Huijbregts, C., 1978. Mining Geostatistics, Academic Press, San Diego, 600.

Kolasa, J., and S. T. A. Pickett, editors., 1991. Ecological heterogeneity. Springer-Verlag, New York, New York, USA.

Li, H., 1990. Spatio-temporal pattern analysis of managed forest landscapes: a simulation approach. Ph.D. Thesis, Oregon State University, Corvallis. 166 pp.

Li, H., Reynolds, J. F., 1994. A simulation experiment to quantify spatial heterogeneity in categorical maps. Ecology, 75(8): 2446-2455.

Matsushita, B., Yang, W., Chen, J., 2007. Sensitivity of the Enhanced Vegetation Index (EVI) and Normalized Difference Vegetation Index (NDVI) to topographic effect: A case study in high-density cypress forest. Sensors, 7:2636-2651.

McGarigal, K, Cushman, S., Neel M., and Ene, E., 2002. FRAGSTATS: Spatial Pattern Analysis Program for Categorical Maps. Computer Software Program. Amherst. http://www.umass.edu/landeco/research/fragstats/fragstats.html.

O'Neill, R. V., Krummel, J. R., Gardner, R. H., Sugihara, G., Jackson, B., DeAngelis, D. L., Milne, B. T., Turner, M. G., Zygmunt, B., Christensen, S. W., Dale, V. H., and Graham, R. L., 1988. Indices of landscape pattern. Landscape Ecology, 1:153-162.

O'Neill, R. V., Gardner, R. H., Sugihara, G., Milne, B. T., Turner, M. G., and Jackson, B., 1991. Heterogeneity and spatial hierarchies. Ecological heterogeneity, 85-96 Springer-Verlag, New York, USA.

Risser, P. G., Karr, J. R., and Forman, R. T. T., 1984. Landscape Ecology: Directions and Approaches. Illinois Natural History Survey, Special Publication 2, Champaign. 18.

Saepuloh, A., Koike, K., Omura, M., Iguchi, M., and Setiawan, A., 2010. SAR- and gravity change-based characterization of the distribution pattern of pyroclastic flow deposits at Mt. Merapi during the past 10 years. Bull.Volcano., 72:221–232.

Sellers, P., 1985. Canopy reflectance, photosynthesis and transpiration. Int. J. Remote Sens., 6: 1335–1372.

Stefanov, W., Ramsey, M., Christensen, P., 2001. Monitoring urban land cover change: an expert system approach to land cover classification of semiarid to arid urban center. Remote Sensing of Environment, 77: 173-185.

Tang, H., Jia, H., Hu, X., Li, D., Xiong, C., 2010. Characteristics of landslides induced by the great Wenchuan earthquake. Journal of Earth Science, 21: 104-113.

Tilman, D. 1982. Resource competition and community structure. Princeton University Press, Princeton. New Jersey.

Tucker, C. J., 1979. Red and photographic infrared linear combinations for monitoring vegetation. Remote Sensing of Environment, 8(2):127-150.

Turner, M. G., 1989. Landscape ecology: the effect of pattern on process. Annual Review of Ecology and Systematics, 20:171-197.

Turner, M. G., 1990. Spatial and temporal analysis of landscape patterns. Landscape Ecology, 4:21-30.

Turner, M. G., and Gardner, R. H., 1991. Quantitative Methods in Landscape Ecology. Springer, New York.

Walsh, S.J., Butler, D.R., Brown, D.G., Bian, L., 1994. Form and pattern of alpine environments: an integrative approach to spatial analysis and modeling in Glacier National Park, USA. In: Heywood, D.I., Price, M.F. (Eds.), Mountain Environments and GIS. Taylor and Francis, London, 189 – 672.

Wilson, E., Hurd, J., Civco, D., 2003. Development of a geospatial model to quantify, describe and map urban growth. Remote Sensing of Environment, 86: 275-285.

# Chapter 6

# Conclusion

## 6.1. Main Conclusion

The whole dissertation is mainly about the work as follows: relationship between earthquake-induced vegetation change and distribution of fracture zones; vegetation distribution and its relationship to fracture zones; quantification of spatial heterogeneity of vegetation, a complement for vegetation pattern.

To characterize the fracture zones, a segment tracing algorithm for automatic lineament extraction from a shaded DEM image was applied to the Yingxiu area, which is situated near the epicenter of Wenchuan earthquake. As the result, three major fracture zones trending NE-SW with the strike of N30-50°E were detected, namely Pitiaohe, Gengda and Yingxiu Faults, from northwest to southeast.

The destructed vegetation was identified by NDVI change resulted from Wenchuan earthquake. According to the result, the destructed vegetations were generally consistent with the fracture zones. Moreover, the distribution of the ruined areas corresponds with the accordant junction of the watersheds. The elevation and distance from the epicenter may be important factors controlling the distribution of the destructed areas of the vegetation induced by the earthquake. The distributions of the areas suffering from severe vegetation destruction were generally consistent with those of the fracture zones. The most severely damaged areas were located around the epicenter and spread toward the west and northwest to Gengda Fault. This fault may have functioned as a shield weakening the earthquake energy. The less severely destroyed areas lied around Pitiaohe Fault, located to the west of Gengda Fault. This fault was relatively far from the epicenter and this indicates that less earthquake energy was received in this area.

NDVI on two dates were employed to represent vegetation and to be analyzed with lineament. Results show that values around either side of main fault are quite different, but appeared to be same trend along the fault, which initially indicate that vegetation cover type around the fracture zones might be different.

Analysis of vegetation type and lineament density showed that broad-leaved forest, mixed forest and farmland persisted in the areas with a moderate level of lineament density and deciduous broad-leaved forest and coniferous forest persisted in the less fractured areas. The relationship between the distributions of shrub and meadow and the lineament density was unclear. Meadow, farmland, shrub persisted in the strongly fractured areas.

Semivariograms of NDVI calculated from ETM (+) images were employed to quantify the variability of the vegetation change before and after the earthquake, and to further examine the relationship between fracture zones and vegetation pattern. Based on the sill values of semivariograms, the spatial heterogeneity of vegetation cover was found to increase after the earthquake. This can be attributed to vegetation fragmentation caused by the earthquake. To examine whether the fracture zones affected the vegetation pattern, two typical areas, which both included one river and one fault, with dimensions of 7×7 km, were selected. The trend of vegetation pattern identified from the anisotropy of NDVI semivariograms shows that the most continuous directions were northeast in both areas, which was consistent with those of the strikes of fracture zones in the two areas.

The emphasis of chapter was placed on the quantification of the spatial heterogeneity and analysis of its changes disturbed by the earthquake. The research was conducted in tow aspects; categorical map and numerical maps.

Vegetation map before and after the earthquake were produced to be the basis data for quantifying spatial heterogeneity in term of categorical map. Ten landscape metrics were selected to quantify the SH in both class-level and landscape-level. The results from class-level indicated that forests get the most fragmentation due to the earthquake. Results from landscape-level revealed that the effect of earthquake on the spatial heterogeneity was obvious; the whole landscape tend to be more heterogeneity, the dominance decreased, and patch shape after the earthquake inclined to be more irregular.

NDVI semivariograms were used to quantify the spatial heterogeneity in terms of the variability of change and spatial structure. It can be concluded from the result that the Wenchuan earthquake caused twice variability than before. Due to lots of vegetation changing to be bare land, range of the NDVI semivarigram increased after the earthquake.

## 6.2. Future Works

Future work will be mainly emphasized on the scale-dependent spatial heterogeneity of vegetation. The form and composition of the alpine environment may be the result of a composite of interacting processes that operate across a range of spatial scales. Relationships observed at a single spatial scale may not be generalizable across spatial scales, and the patterns are dependent upon the scale of observation. It is important to know the scale dependence of processes that determine landscape structure and how the degree and nature of the relationship between pattern and process change with variations in the scale of measurement. Various remote sensing images with different resolution from finer to coarser are available for such study. As for the method, both landscape metrics and semivariogram will be employed. Many landscape metrics are sensitive to scale.

Measurement of landscape metrics across a range of scale could help to find the Knee Point where hierarchical phenomena might exist. Semivariogram can measure the structure of landscape well. We expect to clarify the spatial heterogeneity by integrating landscape metrics and semivariogram.